JOURNAL OF PETROLOGY | VOLUME 55 | NUMBER 7 | PAGES 1429–1456 | 2014 | doi:10.1093/petrology/egu029

Multiple Metamorphic Stages within an Eclogite-facies Terrane (Sesia Zone, Western Alps) Revealed by Th–U–Pb Petrochronology

D. REGIS[1]*, D. RUBATTO[2], J. DARLING[3], B. CENKI-TOK[4], M. ZUCALI[5] AND M. ENGI[1]

[1]INSTITUT FÜR GEOLOGIE, UNIVERSITY OF BERN, BALTZERSTRASSE 1+3, 3012 BERN, SWITZERLAND

[2]RESEARCH SCHOOL OF EARTH SCIENCES, AUSTRALIAN NATIONAL UNIVERSITY, MILLS ROAD, CANBERRA, ACT 0200, AUSTRALIA

[3]SCHOOL OF EARTH AND ENVIRONMENTAL SCIENCES, UNIVERSITY OF PORTSMOUTH, BURNABY BUILDING, PORTSMOUTH PO1 3QL, UK

[4]GÉOSCIENCES MONTPELLIER, UNIVERSITY OF MONTPELLIER 2, UMR 5243, PLACE E. BATAILLON, 34095 MONTPELLIER, FRANCE

[5]DIPARTIMENTO DI SCIENZE DELLA TERRA 'ARDITO DESIO', UNIVERSITÀ DEGLI STUDI DI MILANO, VIA MANGIAGALLI 34, I-20133 MILANO, ITALY

RECEIVED MARCH 2, 2013; ACCEPTED MAY 14, 2014

Convergent plate margins typically experience a transition from subduction to collision dynamics as massive continental blocks enter the subduction channel. Studies of high-pressure rocks indicate that tectonic fragments are rapidly exhumed from eclogite facies to mid-crustal levels, but the details of such dynamics are controversial. To understand the dynamics of a subduction channel we report the results of a petrochronological study from the central Sesia Zone, a key element of the internal Western Alps. This comprises two polymetamorphic basement complexes (Eclogitic Micaschist Complex and Gneiss Minuti Complex) and a thin, dismembered cover sequence (Scalaro Unit) associated with pre-Alpine metagabbros and metasediments (Bonze Unit). Structurally controlled samples from three of these units (Eclogitic Micaschist Complex and Scalaro–Bonze Units) yield unequivocal petrological and geochronological evidence of two distinct high-pressure stages. Ages (U–Th–Pb) of growth zones in accessory allanite and zircon, combined with inclusion and textural relationships, can be tied to the multi-stage evolution of single samples. Two independent tectono-metamorphic 'slices' showing a coherent metamorphic evolution during a given time interval have been recognized: the Fondo slice (which includes Scalaro and Bonze rocks) and the Druer slice (belonging to the Eclogitic Micaschist Complex). The new data indicate separate stages of deformation at eclogite-facies conditions for each recognized independent kilometer-sized tectono-metamorphic slice, between ~85 and 60 Ma, with evidence of intermittent decompression ($\Delta P \sim 0{\cdot}5$ GPa) within only the Fondo slice. The evolution path of the Druer slice indicates a different P–T–time evolution with prolonged eclogite-facies metamorphism between ~85 and 75 Ma. Our approach, combining structural, petrological and geochronological techniques, yields field-based constraints on the duration and rates of dynamics within a subduction channel.

KEY WORDS: *pressure cycles; Sesia Zone; subduction channel; tectono-metamorphic slice; yo-yo subduction*

INTRODUCTION

Exposed high-pressure (HP) crustal rocks in Phanerozoic orogens represent the result of a sequence of processes that

*Corresponding author. Present address: Department of Environment, Earth and Ecosystems, The Open University, Walton Hall, Milton Keynes MK7 6AA, UK. E-mail: daniele.regis@open.ac.uk, regis@geo.unibe.ch

operate at lithosphere scale (i.e. rifting, subduction–accretion, tectonic mixing, return flow–exhumation). The dynamics of assembly of HP and UHP (ultrahigh-pressure) terranes is central to the tectonic study of collision zones. Despite much interest, the mechanisms by which HP rocks descend to mantle depths and then return to the surface remain controversial.

For any given HP–UHP terrane (e.g. Western Alps, Himalaya and Dabie-Shan), exhumation mechanisms are inferred from concepts derived from geological data, notably structural data and pressure–temperature–time (P–T–t) paths, combined with insights derived from numerical and analogue models. Efforts to understand the mechanical behaviour of the lithosphere have singled out several mechanisms in the transition from a subduction to an exhumation stage (e.g. Warren *et al.*, 2008). These mechanisms can be grouped into those driven by buoyancy forces (e.g. Ernst, 2001) and those driven by a range of different tectonic processes (e.g. Platt, 1993; Kurz & Froitzheim, 2002).

Structural and P–T–t data from several HP terranes suggest two separate stages of exhumation: a first rapid stage from mantle to lower crustal levels and a slower exhumation to the surface (Terry *et al.*, 2000; Rubatto & Hermann, 2001; Carswell *et al.*, 2003; Mukherjee *et al.*, 2003; Parrish *et al.*, 2006). Although various mechanisms may operate at different depths, buoyancy forces related to the density contrast are commonly inferred to be particularly significant for the first stage of exhumation, whereas the second stage can be accomplished by a variety of syn- to post-convergent processes (e.g. Ernst, 2001). Moreover, some numerical models invoke extensive tectonic mixing during the subduction and exhumation stages (Gerya *et al.*, 2002; Stoeckhert & Gerya, 2005; Roda *et al.*, 2012), suggesting complex P–T–time paths for lithospheric fragments within a subduction channel.

In comparing P–T data from HP terranes with model predictions several questions arise, such as the following. Under which conditions do fragments from the subducting plate accrete to form an HP terrane? What temporal and spatial scales of tectonic mixing in the subduction channel are realistic? What triggers exhumation and at what rates does it occur?

The dynamics in a subduction channel leading to a specific HP terrane are bound to be complex. For example, results presented by Rubatto *et al.* (2011) have already established the existence of HP cycles for the specific case of the Sesia Zone. To corroborate this complex evolution and quantify it in detail, we adopted an integrative approach that links observations and data across a range of scales, from structural patterns at kilometer scale in the field down to petrological and chronological data obtained at micrometer scale. This field-based study of a significant portion of the Sesia Zone reveals a multi-stage evolution of this HP continental terrane, from subduction to exhumation. Careful structural control in sampling and detailed petrography were used to select samples for petrochronology to arrive at a coherent interpretation of the P–T–t data in the context of subduction dynamics. Accessory phases proved most useful in deducing parts of the metamorphic reaction history and to relate the specific stages of the evolution. Microbeam Th–U–Pb geochronology by sensitive high-resolution ion microprobe (SHRIMP) and laser ablation inductively coupled plasma mass spectrometry (LA-ICP-MS) allowed dating of these stages. Single grain (or subgrain) dating turned out to be essential to utilize the preserved fine detail of (over)growths within each accessory mineral. Where possible, mineral chronometers were combined to exploit their capacity to record different stages of the metamorphic evolution. Particular attention was paid to the distribution of rare earth elements (REE) between major metamorphic minerals and the accessory phases used for geochronology (zircon and allanite) to gain additional insight into the relative timing of accessory and major mineral growth (e.g. Hermann & Rubatto, 2003; Gabudianu Radulescu *et al.*, 2009). Two independent tectono-metamorphic 'slices' (termed the Druer and Fondo slices, respectively) were recognized within the Sesia Zone because they followed different P–T–t paths within the subduction channel. Independent mobility of these slices has been unequivocally demonstrated because they underwent different P–T conditions at the same time. The results obtained on the P–T–t evolution of each tectono-metamorphic slice are used to estimate the rates of subduction and exhumation.

GEOLOGICAL BACKGROUND AND SAMPLING STRATEGY

The Alps are a double-vergent orogen that formed as a result of the convergence between the European and African (Apulia) tectonic plates (e.g. Dewey *et al.*, 1989). The Sesia Zone (SZ) is the largest exposed slice of Apulian continental crust in the Western Alps that underwent subduction prior to the Alpine orogeny and extensively preserves eclogite-facies assemblages. It has traditionally been divided into three subunits (from west to east, Fig. 1a, Table 1): the Gneiss Minuti Complex (GMC), the Second Dioritic–Kinzigitic Zone (IIDK), and the Eclogitic Micaschist Complex (EMC). These tectonic complexes consist of a metasedimentary basement composed of Variscan amphibolite-facies rocks intruded by late Variscan granitoids that experienced polyphase tectono-metamorphic reworking during the Alpine orogeny (Dal Piaz *et al.* 1972; Compagnoni, 1977; Compagnoni *et al.*, 1977; Gosso, 1977; Lardeaux & Spalla, 1991). The three units preserve to different degrees an early HP imprint (peak pressures of 1·0–1·5, 1·0–1·2, and 1·6–2·4 GPa respectively) that partially re-equilibrated under greenschist-facies conditions

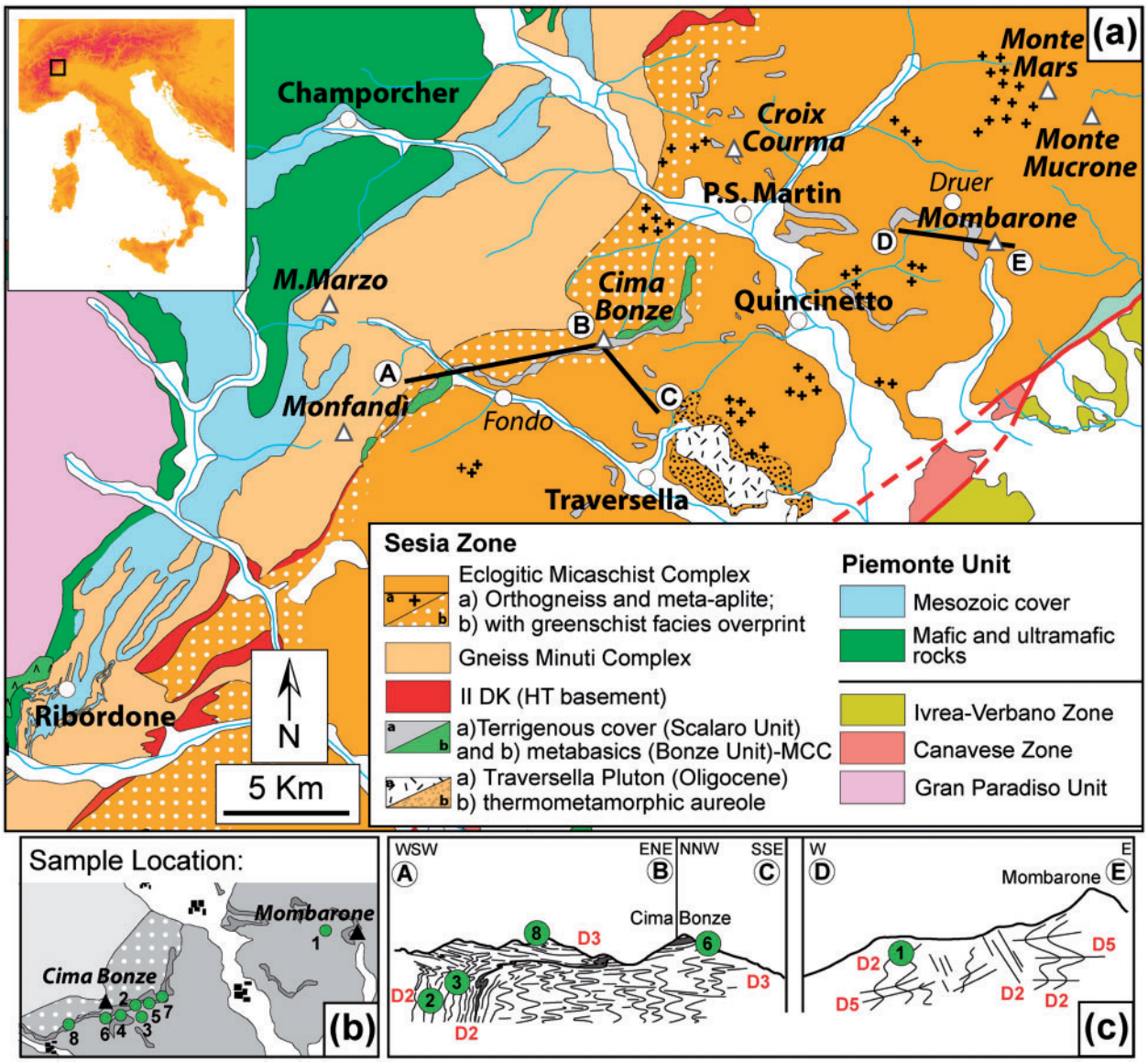

Fig. 1. (a) Geological map of the central Sesia Zone (SZ), Western Italian Alps. Greenschist-facies overprinted portion of the Eclogitic Micaschist Complex (EMC) corresponds to the Intermediate Unit of Venturini (1995). (b) Location of the studied samples; numbers refer to sample numbers in Table 2. (c) Samples shown in their appropriate structural position (from out-of-section location); D_3-related quartzite samples Nos 4, 5, and 7 are not shown on the map. Cima Bonze profile is modified after Babist *et al.* (2006); Mombarone profile is modified after Zucali (2002). It should be noted that (a), (b) and (c) are at different scales.

(Dal Piaz *et al.*, 1972; Compagnoni *et al.*, 1977; Gosso, 1977; Lardeaux *et al.*, 1982; Vuichard, 1989; Zucali *et al.*, 2002; Tropper & Essene, 2002). An alternative subdivision of the Sesia Zone has recently been proposed by Babist *et al.* (2006) on the basis of regional structural maps and correlations (Table 1); the polyphase deformation patterns documented therein provide the basis for the sampling strategy in the present study.

Venturini (1995) identified a monometamorphic cover complex (MCC; Fig. 1a, Table 1) largely situated between the internal (EMC) and the external (GMC) complexes. This cover sequence comprises terrigenous and carbonate metasediments (Scalaro Unit) associated with mafic rocks and subordinate quartz-rich metasediments (Bonze Unit). As the majority of the rocks belonging to the 'monometamorphic' cover are actually polymetamorphic (e.g. Rubatto *et al.* 1999), the acronym MCC is not used in the present study. When referring to the monometamorphic metasediments alone, the term Scalaro Unit is used instead and, to avoid confusion, the term Bonze Unit refers to the complex of polymetamorphic mafic rocks and associated metasediments.

Table 1: Correlation of the different names used in the literature for the tectonic complexes and units of the Sesia Zone

	Tectonic Units and Terms				
	Compagnoni et al. (1977)	Venturini (1995)	Babist et al. (2006)	*This study*	
Sesia Zone (formerly also called Sesia-Lanzo Zone) (part of the Austroalpine Domain)	EMC	EMC	Mombarone Nappe	EMC → Druer tectonometamorphic slice	Not to scale
		MCC* → Scalaro Unit* / Bonze Unit*	Bonze Unit*	Scalaro Unit* / Bonze Unit → Fondo tectonometamorphic slice	
	GMC	Intermediate unit	Bard Nappe	Intermediate unit	
		GMC		GMC	
	IIDK	IIDK	IIDK	IIDK	

EMC, Eclogitic Micaschist Complex; GMC, Gneiss Minuti Complex; IIDK, Second Dioritic–Kinzigitic Zone; MCC, Monometamorphic Cover Complex.
*Monometamorphic units.

Previous geochronological studies of the Sesia Zone (SZ) have mainly focused on the age of the HP Alpine metamorphism. A widely accepted age for this stage is ~65 Ma based on data obtained using a number of geochronological methods (e.g. U–Pb, Rubatto *et al.*, 1999; Rb–Sr, Inger *et al.*, 1996; Ar–Ar, Venturini, 1995; Lu–Hf, Duchêne *et al.*, 1997). However, these studies also recognized several problems, notably those linked to excess argon (e.g. in phengite), and partial thermal resetting of some systems. When considering all the studies jointly, it appears that the Alpine high-pressure stage(s) may span a time interval of more than 30 Myr across the EMC from ~90 Ma to ~60 Ma (e.g. Hunziker, 1974; Oberhänsli *et al.*, 1985; Stoeckhert *et al.*, 1986; Venturini, 1995). Recently, this range in the apparent ages of the HP assemblages has been reframed in the context of two distinct episodes of high-pressure metamorphism, at ~79–75 Ma and ~70–65 Ma, separated by a short-lived period of exhumation (Rubatto *et al.*, 2011).

To substantiate and further quantify the multiple HP stages proposed by Rubatto *et al.* (2011), this study presents an expanded dataset with new petrographic observations, mineral chemistry of major and accessory phases, their microtextural relations and subgrain-scale geochronology ('petrochronology') for several samples from the central SZ and new data for the Mombarone area. The tectonic scenario proposed by Zucali *et al.* (2002) and Babist *et al.* (2006) provided the basis for a focus on specific parts of the poly-deformed complexes. Structurally controlled sampling (Fig. 1b and c) was performed on polycyclic rocks of the Eclogitic Micaschist Complex and on both mono- and polycyclic samples belonging to the Scalaro and Bonze Units. On the basis of the new data, two tectono-metamorphic slices have been recognized in the central SZ. In this study, the term Druer slice (Dr) is used to denote a slice (named after the Druer cabin, Val d'Aosta, Fig. 1a) formed by EMC rocks in the Mombarone area (Table 1). Its size cannot be precisely delimited. Until future studies provide evidence of internal differences, the central part of the EMC (i.e. the Druer slice documented here) is viewed as a single tectono-metamorphic unit. The unit package formed by the Scalaro and Bonze rocks, which shows a coherent *P–T–t* evolution, represents another slice that surfaces in the central Sesia Zone (Table 1). To avoid confusion, this tectono-metamorphic slice is referred to as the Fondo slice (after the town of Fondo, Val Chiusella, Fig. 1a).

ANALYTICAL METHODS

Whole-rock major element compositions

Major element compositions were determined by X-ray fluorescence (XRF) analysis at the University of Fribourg (Switzerland) and at Actlabs (Activation Laboratories) Ltd. (Canada). Whole-rock analyses were made of ~1 kg samples, which were crushed and pulverized. Loss on ignition (LOI) was determined by weight difference after heating to 1050°C for 15 h.

Imaging and electron microprobe analysis (EMPA)

Electron microprobe analysis (EMPA) on major and REE minerals was performed on polished thin sections using a Jeol JXA8200 electron microprobe at the University of Bern. Operating conditions were set to 15 kV and 20 nA (spot size ~1 μm) for major minerals and 25 kV and 50 nA (spot size 3 μm) for all the REE minerals. The matrix correction used is φ(ρZ), based on Armstrong (1988, 1991). A selection of natural and synthetic standards was used: $La_{0·95}Nd_{0·05}TiO_3$ (La), $NdGaO_3$ (Nd), Y_2O_3 (Y), $PbCrO_4$ (Pb), huttonite (Th), UO_2 (U), spinel (Al, Mg), wollastonite (Si, Ca), albite (Na), ilmenite (Ti), monazite std (Ce, P), SmP_5O_{14} (Sm), PrP_5O_{14} (Pr), GdP_5O_{14} (Gd), tephroite (Mn), DyP_5O_{14} (Dy), almandine (Fe), celestine (Sr), HoP_5O_{14} (Ho), ErP_5O_{14} (Er), TbP_5O_{14} (Tb) and YbP_5O_{14} (Yb). The procedure for REE minerals, described in detail by Scherrer *et al.* (2000), was refined by Janots *et al.* (2008). X-ray elemental maps were obtained for Ce, Ca, Y, La, Mg, Mn, Nd, Sr and Th in allanite and clinozoisite, using the electron microprobe with a beam set at 25 kV and 50 nA. Step size was 0·5 μm and dwell time per pixel was 40–60 ms. Back-scattered electron (BSE) images were obtained with a Zeiss EVO50 scanning electron microscope (SEM; University of Bern) using a voltage of 20 kV, current of ~1 nA and a working distance of 10 mm.

Mineral LA-ICP-MS trace element analysis

Trace element analysis of allanite, zircon and garnet was performed by LA-ICP-MS at the Institute of Geological Sciences, University of Bern, utilizing a Geolas Pro 193 nm ArF excimer laser coupled to an Elan DRC-e ICP-MS system. Laser beam diameters ranged from 16 to 44 μm, with an energy density on the sample of 7 J cm^{-2}. A He–H_2 gas mixture was used as the aerosol transport gas. Sample analyses were calibrated using NIST SRM 612, and corrected using internal standards (Al for allanite and garnet—EMPA, and stoichiometric Si for zircon). Data reduction was performed using the SILLS software package (Guillong *et al.*, 2008). Accuracy was monitored using NIST SRM 610 and NIST SRM 614, which yield average values within uncertainty of the reference values (Horn *et al.*, 1997; Pearce *et al.*, 1997)

Mineral separation and ion microprobe dating of accessory minerals

Samples were disaggregated using a SELFRAG apparatus (University of Bern) to a grain size of <250 μm. Zircon grains were separated using conventional magnetic and density-based techniques, mounted in epoxy resin and

polished down to expose their near equatorial section. Cathodoluminescence (CL) imaging of zircon was carried out on a Hitachi S2250N SEM fitted with an ellipsoidal mirror for CL at the Electron Microscopy Unit at the Australian National University in Canberra. Operating conditions for the SEM were 15 kV, 60 μA and 20 mm working distance. Back-scattered electron images of allanite were obtained with a Cambridge S360 SEM working at 15 kV, ~2 nA and a working distance of ~17 mm.

Zircon and allanite were analyzed for U, Th and Pb using the sensitive high-resolution ion microprobe (SHRIMP II) at the Australian National University in Canberra. For zircon, instrumental conditions and data acquisition were generally as described by Williams (1998). The data were collected in sets of six scans throughout the masses, and a reference zircon was analyzed every fourth analysis. The measured $^{206}Pb/^{238}U$ value was corrected using reference zircon from the Temora granodiorite (TEM; Black *et al.*, 2003). The fraction of non-radiogenic ^{206}Pb (f_{206}) was calculated from the measured $^{207}Pb/^{206}Pb$ ($^{7/6}Rm$) and the non-radiogenic $^{207}Pb/^{206}Pb$ ($^{7/6}Rc$) according to Williams (1998); that is, $f_{206} = (^{7/6}Rm - {}^{7/6}R*)/(^{7/6}Rc - {}^{7/6}R*)$, where $^{7/6}R*$ is the expected radiogenic $^{207}Pb/^{206}Pb$ assuming concordance at the approximate age of the sample. The $^{7/6}Rc$ composition was based on the Stacey & Kramers (1975) model.

For allanite, instrumental conditions and data acquisition were as described by Gregory *et al.* (2007), with isotope data collected from sets of six scans through the masses. Th–U–Pb allanite data were collected over multiple analytical sessions with calibration errors of 1·5–2·0 % (2σ), which were propagated to single analyses. The measured $^{208}Pb/^{232}Th$ value was corrected using the allanite standard TARA (417 Ma; Gregory *et al.*, 2007). A secondary standard (Bona; $^{208}Pb/^{232}Th$ age of 30·1 Ma; von Blanckenburg, 1992) returned ages within 1% of the nominal value. To account for any additional uncertainty owing to matrix effects (standard and unknown can be significantly different in composition), the uncertainty on average ages was forced to be at least 2%.

All allanite analyses were corrected for common Pb on the basis of measured $^{207}Pb/^{206}Pb$ in a similar way to zircon, as described by Gregory *et al.* (2007). Common Pb measured in allanite is essentially inherent, therefore an estimate of the initial Pb composition at the time of crystallization from an evolving model Pb composition (Stacey & Kramers, 1975) was assumed. This assumption was justified by applying free regressions to the uncorrected data. One example is shown in the text for the allanite rims of sample bva0840 (No. 1, Table 2); the Tera–Wasserburg initial $^{207}Pb/^{206}Pb$ intercept of 0·8417 ± 0·014 (2σ) of the analyses is within error of the model Pb compositions at ~85 Ma. Direct measurement of the common Pb composition by LA-ICP-MS in other minerals in the sample (see below) further confirmed that the composition is within error of the Stacey & Kramers (1975) model.

A 2D Th isochron normalized to common ^{206}Pb (Gregory *et al.*, 2007) was used to further test the assumption of initial Pb and age robustness. In all cases the isochron method returned ages within error of the average $^{208}Pb/^{232}Th$ age; as a result of the small range in $^{232}Th/^{206}Pb$ within the data, the isochron ages generally have larger uncertainties.

For both zircon and allanite, the data evaluation and age calculation were carried out using the software Squid (Squid 1 for zircon and Squid 2 for allanite) and Isoplot/Ex (Ludwig, 2003), respectively. Average ages are quoted at 95% confidence level (CL).

The Th–U–Pb geochronology of allanite by LA-ICP-MS

Analyses were undertaken at the University of Portsmouth, using a New Wave 213 nm Nd:YAG laser coupled with an Agilent 7500cs ICP-MS. Analytical protocols and instrument conditions have been described in detail by Darling *et al.* (2012*a*). Key points of the method are: (1) line-raster ablation to minimize time-dependent elemental fractionation; (2) external normalization to the zircon standard Plešovice (Sláma *et al.*, 2008); (3) the use of measured ^{204}Pb to correct for inherited common-Pb. Accuracy was monitored via analyses of the Tara allanite, which yielded weighted-mean common-Pb corrected $^{206}Pb/^{238}U$ and $^{208}Pb/^{232}Th$ ages of 424 ± 13 Ma ($n = 11$; MSWD = 1·5) and 416·4 ± 1·9 Ma (MSWD = 1·02) respectively, which are within uncertainty of previously published values (Gregory *et al.*, 2007).

To aid common-Pb correction of Th–U–Pb isotope analyses, Pb isotopes were measured in feldspar, pyrite and white-mica from sample bva0840 (No. 1, Table 2). Analytical protocols followed those described by Darling *et al.* (2012*b*).

SAMPLE DESCRIPTION AND MINERAL CHEMISTRY

Microprobe (major element) and LA-ICP-MS (trace element) geochemical data are reported in Supplementary Data: Electronic Appendix 2 (Mineral Chemistry) and Electronic Appendix 3 (Trace Elements). Supplementary data are available for downloading at http://www.petrology.oxfordjournals.org.

Druer tectono-metamorphic slice

Chloritoid–kyanite–garnet mica schists (e.g. sample No. 1, Table 2) were chosen for detailed investigation from a larger collection of potentially suitable samples because they contain datable minerals (allanite and zircon) in sufficient amounts and with clear microstructural relations with *P–T*-relevant phases (e.g. phengite). The samples

Table 2: List of the analyzed samples

No.	Sample name	Location	Lithology	Elevation (m a.s.l.)	Latitude and longitude GPS (UTM)
1	bva0840	Mombarone-Druer cabin	Quartz-rich mica schist (ky-cld-grt), polymetamorphic	1817	32T 0412542 5049802
2	bva0926	East of Colle Bonze-Alpe Muanda Superiore	Quartz-rich mica schist (jd-grt), polymetamorphic	2037	32T 0401953 5045123
3	bva0851	East of Colle Bonze-Alpe Muanda Superiore	Metagabbro, polymetamorphic	2040	32T 0401998 5045126
4	bva0824	Cima Bonze	Phengite-rich quartzite monometamorphic	2100	32T 0401949 5044959
5	bva0919	Cima Bonze-Alpi Cima Bracca	Phengite-rich quartzite monometamorphic	1946	32T 0402091 5044966
6	bva0845	Cima Bonze	Phengite-rich quartzite monometamorphic	2426	32T 0401004 5044902
7	bva0861	Scalaro village	Phengite-rich quartzite monometamorphic	1575	32T 0403492 5045332
8	vc0909	Chiusella valley-Alpe Miassa	Phengite-rich quartzite monometamorphic	1845	32T 0399369 5044902

Numbers related to sample names are used in figures and captions. a.s.l., above sea level.

were collected near Colma di Mombarone (Fig. 1b and c, Table 2) at the entrance of the Aosta valley.

In the area sampled, the syn-eclogitic metamorphic (M) and deformational (D) imprint (M_2, D_2) was recognized as the dominant phase (Zucali *et al.*, 2002, 2004; Gatta *et al.*, 2009; Zucali & Spalla, 2011), with isoclinal folds (centimeter- to meter-size) transposing the primary foliation into a new penetrative axial planar foliation (S_2, Fig. 2a), which is marked by the shape preferred orientation (SPO) of Ph-II, Pg, Ky, Cld-II, and Aln. Strong retrograde stage deformation (D_4) led to a discontinuous foliation or shear bands; epidote-blueschist-facies assemblages define this fabric in all the lithologies of the Mombarone area (Zucali *et al.*, 2002). Late D_5 structures form open to isoclinal folds, ranging in size from centimeters to kilometers, with subhorizontal axial planes (Fig. 2a). At greenschist-facies conditions, however, foliation developed only locally.

The mica schists occur as bodies less than 2 m thick and several meters long at the contact with omphacite-rich mica schists; locally they are interbedded with calcite-rich marbles (Fig. 2a). The rocks studied are light grey with porphyroblasts of garnet (centimeter-sized, dark red), chloritoid (millimeter-sized, dark green) and kyanite (centimeter-sized, white), and a pervasive foliation defined by phengite. Microscopically they consist of quartz (40%), phengite–muscovite (15%), paragonite (5%), garnet (15%), kyanite (10%), chloritoid (10%), allanite (3%), chlorite (1%) and accessory rutile, calcite, zircon and Fe-oxides (Fig. 2b and Supplementary Data: Electronic Appendix 1, Fig. S1.1). Kyanite grains have homogeneous cores and symplectitic rims of quartz and kyanite suggesting two metamorphic stages of growth (Gatta *et al.*, 2009). Minerals do not show evidence of strong deformation. Only in few samples it is possible to observe wavy extinction and kinking of micas, as well as fragmentation of the more competent phases. Allanite forms large crystals (~1 cm) in close microstructural relationship with phengite and paragonite, garnet, kyanite and chloritoid. In all the investigated samples, allanite is associated with phengite (marking the the S_2 foliation) and shows sharp grain boundaries with garnet, kyanite and chloritoid, thus indicating simultaneous crystallization of this assemblage. Moreover, allanite is included in garnet rims (Supplementary Data: Electronic Appendix 1, Fig. S1.5) and includes small phengite crystals.

In the samples analyzed, garnet is almandine-rich ($X_{alm} = 0{\cdot}67–0{\cdot}70$) with a uniform grossular content (0·15–0·18) and slight zoning in spessartine (core to rim: 0·06–0·02). Trace element compositions of garnet show a decrease in total REE from core to rim (Supplementary Data: Electronic Appendix 1). Across the entire grain, garnet is characterized by a flat pattern in the middle REE (MREE; $Dy_N/Gd_N = 1{\cdot}2–1{\cdot}8$) to heavy REE (HREE; $Dy_N/Yb_N = 0{\cdot}9–1$) at about 50–100 times chondrite (Supplementary Data: Electronic Appendix 1) with rims having slightly lower REE contents than cores.

Micas are characterized by variable amounts of celadonite substitution depending on the microstructural site. High-pressure phengite (Ph-II, coexisting with paragonite, Supplementary Data: Electronic Appendix 1, Fig. S1.2) has Si contents of 3·19–3·21 a.p.f.u. Muscovite (Ms-III) grew at the retrograde stage (D_4–D_5) and shows lower Si contents (3·15–3·17 a.p.f.u). Chloritoid porphyroblasts (Cld-II, $X_{Mg} = 0{\cdot}16–0{\cdot}17$) parallel to the S_2 foliation grew with the HP assemblage. Cld-III ($X_{Mg} = 0{\cdot}11–0{\cdot}14$) grew along fractures and cleavage planes of micas and locally it forms small aggregates (D_5 stage).

Microstructures show that allanite crystals grew as part of the HP assemblage parallel to the main S_2 foliation (Fig. 2b and c). The patchy texture observed in BSE images (Fig. 2c) is related to variations in total REE content, which ranges between 0·3 and 0·5 a.p.f.u. (Fig. 2d). No zoning in major elements was observed. Locally

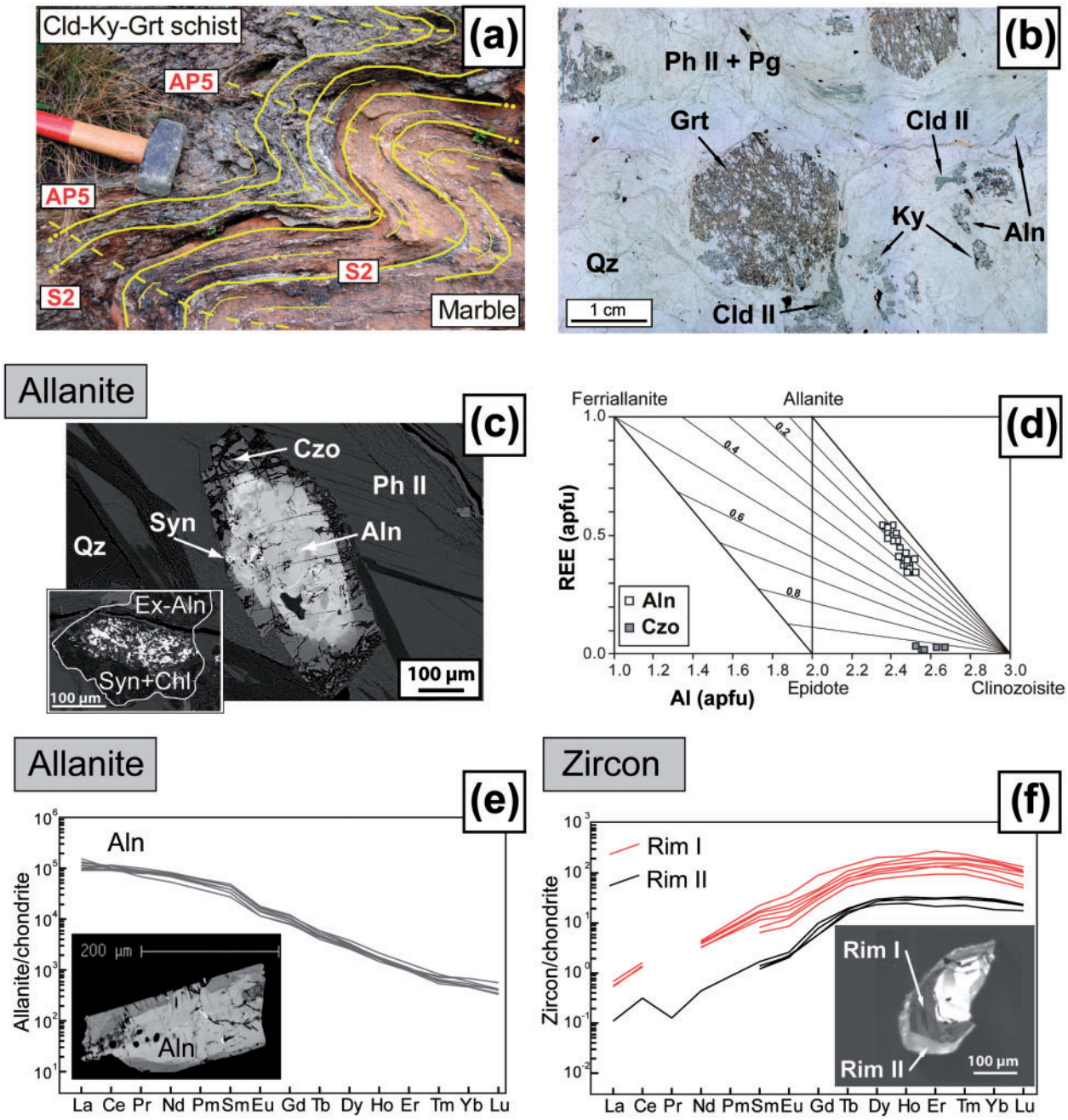

Fig. 2. Polymetamorphic metapelite, EMC. (a) Superimposition of D_5 folds on D_2 structures at the contact between Cld–Ky–Grt mica schists and marbles. D_5 folds are meter-sized open folds with a gently dipping axial plane. AP, Trace of axial plane (AP5). (b) Microstructural relationship between HP minerals; poikiloblastic garnet (Grt) porphyroblasts coexist with chloritoid (Cld), kyanite (Ky), phengite (Ph) + paragonite (Pg), and allanite (Aln) embedded in a quartz (Qz) matrix. It should be noted that allanite crystals are not aligned owing to post-S_2 deformation. Plane-polarized light. Mineral abbreviations used in figures are from Whitney & Evans (2010) with some additions (see Supplementary Data: Electronic Appendix 1). (c) Allanite (Aln) elongated parallel to the S_2 foliation marked by Ph-II. Clinozoisite (Czo) coronae on allanite formed during the D_4 stage. In the inset Aln is replaced by Syn + Chl (D_5). (d) Aln and Czo compositions plotted in a Petrík *et al.* (1995) diagram. (e) Chondrite-normalized REE patterns of allanite show strong enrichment in LREE ($La_N/Lu_N = 270$) and the absence of an Eu anomaly; normalizing values from Sun & McDonough (1989). (f) Chondrite-normalized REE patterns for zircon rims; normalizing values from Sun & McDonough (1989).

allanite is rimmed and partially replaced at a late stage (D_4) by clinozoisite (FeO_{tot} ~7 wt %) overgrowing the S_2 foliation. Allanite displays REE patterns with a strong enrichment in light REE (LREE) (with respect to the HREE) and with no Eu anomaly (Fig. 2e). In the most retrogressed samples, allanite and clinozoisite are replaced by fine-grained chlorite + synchysite [$REECa(CO_3)_2F$] + clay minerals ± apatite (Fig. 2c).

In the analyzed samples, zircon crystals are clear to light yellow and generally euhedral (100–300 μm). Their internal structure is characterized by large cores with oscillatory zoning, overgrown by two distinct rims that do not show regular zoning and differ in CL emission and composition (Fig. 2f). The first rim (rim-I) shows low CL emission and contains more U than the outer rim (rim-II). The two overgrowths also differ in their chemical composition. Rim-I has a higher REE content and both overgrowths have a generally flat HREE pattern at 10–110 times chondrite (Fig. 2f). Rim-I includes small crystals of rutile.

Fondo tectono-metamorphic slice

Structurally controlled samples were collected from both the monocyclic Scalaro Unit and the polycyclic Bonze Unit. Monometamorphic sediments were chosen because they record only the Alpine metamorphism, thus avoiding problems related to a polycyclic history. As the monometamorphic unit occurs in only a limited band of outcrops, suitable polymetamorphic rocks (Bonze Unit) were also investigated. Seven samples (Table 2) were studied in detail: one polymetamorphic metapelite (No. 2, Bonze Unit), one metagabbro (No. 3, Bonze Unit) and five samples of monometamorphic phengite-rich quartzite (Nos 4–8, Scalaro Unit).

Polymetamorphic metapelite (No. 2, Bonze Unit)

The polycyclic metapelites were collected east of Colle Bonze (Fig. 1b, Table 2); they are associated with metagabbros and eclogites (Venturini, 1995). The samples are light green with millimeter-sized garnet porphyroblasts (dark red) and jadeite crystals (light green) in a quartz-rich matrix. Microscopically they consist of quartz (55%), jadeite (25%), phengite (10%), garnet (5%), allanite and epidote (2%), glaucophane (1%), acmite (1%) and accessory rutile, Fe-oxides and zircon (Supplementary Data: Electronic Appendix 1, Fig. S2.1).

In this area Babist *et al.* (2006) recognized an early schistosity (S_1) formed under eclogite-facies conditions. This foliation is overprinted under retrograde blueschist- to greenschist-facies conditions in what those researchers termed fabric domain 2. This overprinting involved mylonitic shearing and isoclinal folding with development of a now vertical foliation (S_2; Fig. 3a).

Microtexturally the metapelites are characterized by a pervasive foliation (S_2; Fig. 3a) marked by phengite wrapping the HP assemblage (M_1: jadeite + garnet + phengite, Fig. 3a). Two generations of garnet were distinguished (Supplementary Data: Electronic Appendix 1, Fig. S2.2): early garnet characterized by a high MnO content (10–11 wt %) and low CaO (~7 wt %) is rimmed by newly formed garnet (Fig. 3a). The latter generation shows a slight decrease in spessartine component from mantle to rim, and uniform contents of almandine (X_{Fe} 0·5–0·55) and grossular (X_{Ca} 0·30–0·35). Garnet is characterized by enrichment in HREE from mantle to rim (Fig. 3b). Clinopyroxene is homogeneous in composition, close to $(Na_{0·93}Ca_{0·07})(Al_{0·89}Fe_{0·1}Mg_{0·01})Si_2O_6$ (Supplementary Data: Electronic Appendix 1, Fig. S2.3). In the more retrogressed samples, jadeite crystals are replaced by albite + sericite and are rimmed by a very thin corona of acmite (X_{Fe} ~0·7). Strongly deformed and kinked micas (Ph-I, Si = 3·22–3·25 a.p.f.u.) are associated with the HP phases. A second generation of mica (Ph-II, Si = 3·25–3·3 a.p.f.u.) marks the S_2 foliation.

Accessory zircons are euhedral. In CL they show inherited cores overgrown by three thin rims. The first of these (rim-I) is characterized by low CL emission and a high U content. It is enriched in HREE (Supplementary Data: Electronic Appendix 1, Fig. S2.8) with a small Eu anomaly (Eu_N/Eu^*_N 0·38) and low Th/U (0·01–0·02). The external rims (rim-II and rim-III) are characterized by low U and Th contents. The first generation (rim-II) shows patchy zoning and abundant HP inclusions (jadeite partially replaced by albite, phengite, epidote, rutile and quartz), whereas rim-III is more homogeneous, with lower CL-emission and no inclusions. Rim-III is only 5–10 μm wide, which implies that most of the analyses (trace elements and age data) obtained represent mixtures of the two outer domains. Despite this, mixed REE analyses indicate that rim-III is slightly depleted in HREE (Yb–Lu) with respect to rim-II (Fig. 3c).

Metagabbro (No. 3, Bonze Unit)

Mafic rocks (mainly metagabbros) associated with the impure quartzites of the Scalaro Unit and polymetamorphic metasediments (No. 2) were investigated (Table 2) because they locally preserve the older fabrics (D_1, D_2) and mineral assemblages. In these rocks the main foliation (S_2), marked by sodic amphibole, clinozoisite ± chlorite, surrounds the HP assemblage (garnet + omphacite + phengite, M_1 stage, Fig. 4a). The S_2 mylonitic foliation was subsequently refolded by D_3 isoclinal folds with subhorizontal axial planes (Fig. 4b). Several structural relics of the magmatic assemblage can be observed in thin section, such as discolored hornblende partially replaced by glaucophane and relics of orthopyroxene (hypersthene).

M_1 garnet is almandine rich (X_{Fe} 0·55), with a uniform grossular content (X_{Ca} 0·3) and shows a weak decrease in spessartine from core to rim (X_{Mn} 0·08–0·01,

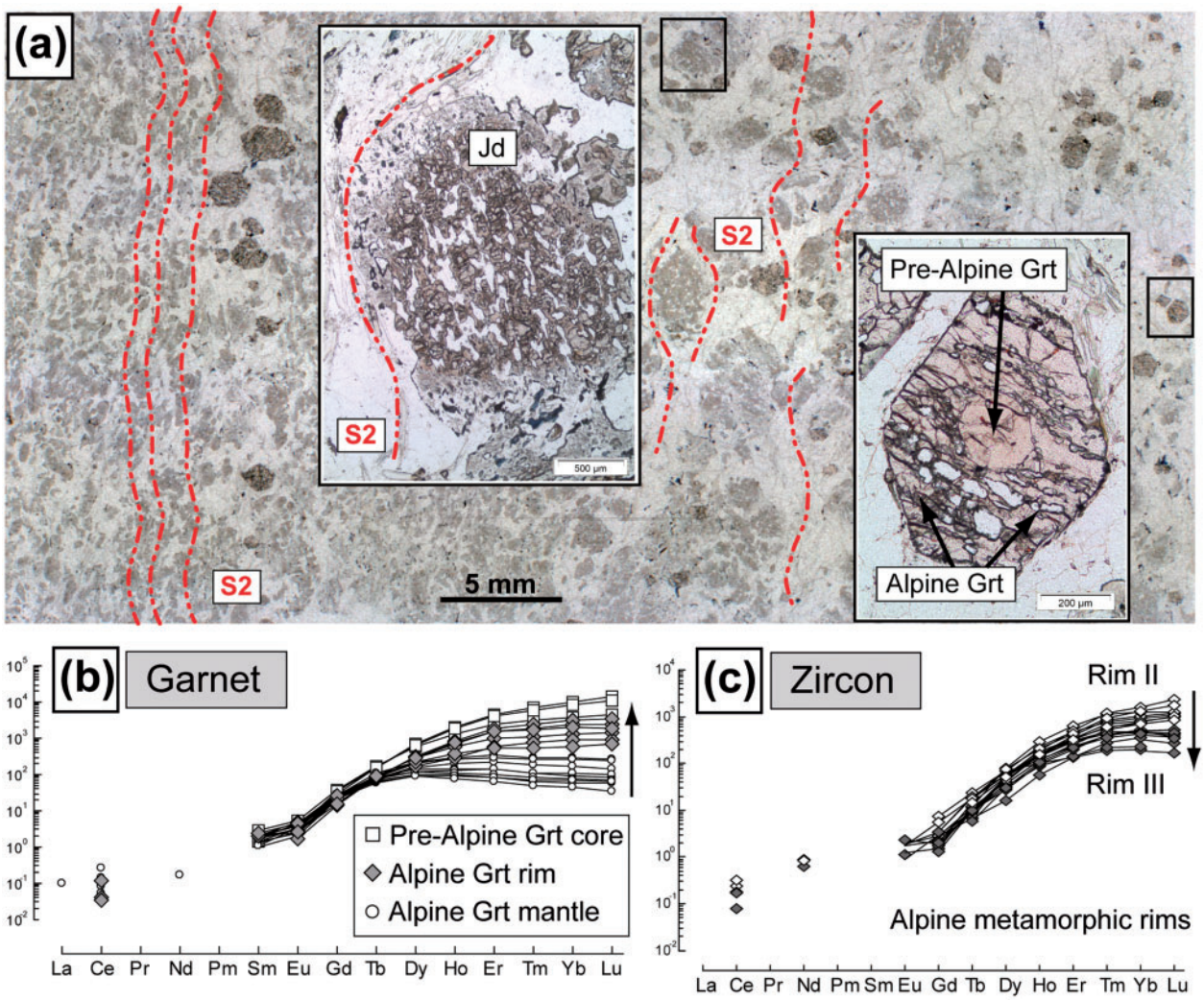

Fig. 3. Polycyclic metapelites, Bonze Unit. (a) Microstructures of Jd–Grt mica schists as seen under an optical microscope. The millimeter-sized garnet (dark red) and jadeite crystals (light green) wrapped by phengite marking the S_2 foliation should be noted. (b) REE patterns of pre-Alpine and Alpine garnets. The latter are characterized by enrichment of MREE and HREE from mantle (depleted in MREE and HREE with $Dy_N/Yb_N \geq 1$) to rim ($Dy_N/Yb_N \leq 1$). (c) REE patterns for zircon rims-II and -III. A minor depletion in HREE is observed in rim-III compared with rim-II. In (b) and (c) normalizing values are from Sun & McDonough (1989).

Supplementary Data: Electronic Appendix 1, Fig S3.2). Clinopyroxene associated with garnet is homogeneous, with a composition close to $(Na_{0\cdot45}Ca_{0\cdot55})(Al_{0\cdot41}Fe_{0\cdot11}Mg_{0\cdot48})Si_2O_6$. Within omphacite and garnet crystals, prograde titanite, clinozoisite ± glaucophane are preserved. Syn-M_1 white micas have phengitic compositions with Si contents ranging between 3·38 and 3·41 a.p.f.u. Glaucophane crystals marking the S_2 mylonitic foliation are overgrown by later amphibole (Act-I, Act-II), which formed together with chlorite, albite ± quartz (Fig. 4d).

Several generations of epidote grew in different microstructural sites. Fe-epidote contents decrease from core to rim in epidote included within garnet and omphacite. Clinozoisite marks the mylonitic foliation (S_2) together with glaucophane (Fig. 4a). Large crystals (0·5–1 mm) of zoisite with characteristic hour-glass (HG) zoning overgrow the S_2 foliation (Fig. 4a and e). Glaucophane and rutile ± titanite are the main phases included in HG-zoisite. Outside the HG sector, zoisite has a relatively homogeneous composition (X_{ep} 0·09–0·1); higher X_{ep} values (0·14–0·17) are reached in the HG zone (Supplementary Data: Electronic Appendix 1, Fig. S3.5). Late clinozoisite overgrowing the HG-zoisite is characterized by enrichment in Fe-epidote contents from core to rim.

Monometamorphic phengite-rich quartzites (Nos 4–8, Scalaro Unit)

As described by Babist *et al.* (2006), the S_2 mylonitic foliation is refolded by isoclinal folds (AP3, Fig. 5a), which led to the development of a pervasive foliation (S_3). The S_3 foliation is

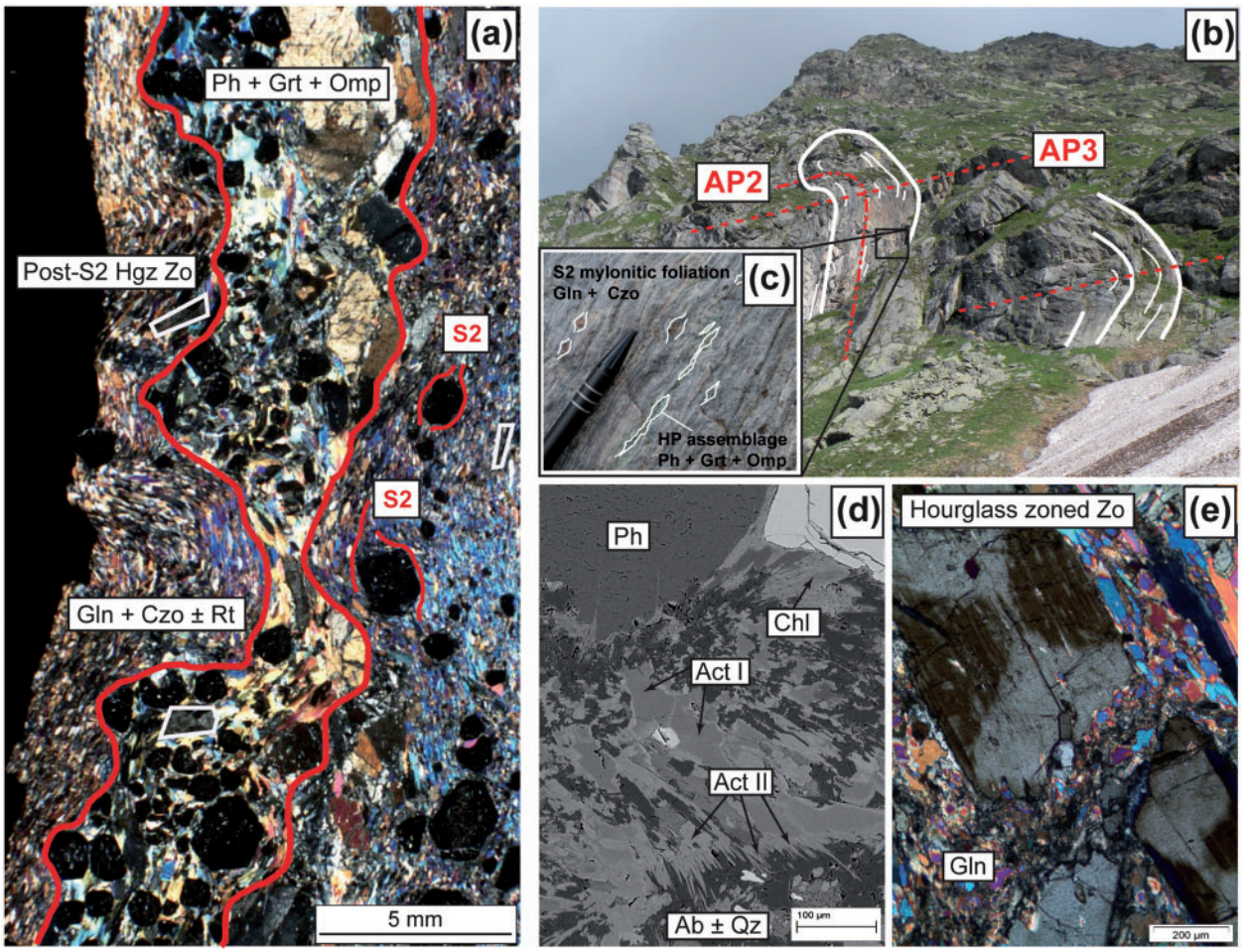

Fig. 4. Metagabbro, Bonze Unit. (a) Photomicrograph showing the relationships between microstructural evolution and mineral growth during D_1, D_2 and D_3 deformation phases. High-pressure domains are wrapped by the blueschist foliation. (b) Superimposition of D_3 onto D_2 folds in metagabbros in the Chiusella valley. In the enlargement (c) HP lenses (Ph + Grt + Omp) and isolated garnets are wrapped by the S_2 mylonitic foliation marked by fine-grained glaucophane (Gln) and clinozoisite (Czo). (d) Actinolite I and II crystals growing during the last stages of exhumation with albite + chlorite + quartz. (e) D_3-related hour-glass zoned zoisite overgrowing the S_2 foliation.

particularly well developed in impure quartzites (Scalaro Unit), where it is marked by phengite (Fig. 5b). The samples consist of quartz (60%), phengite (20%), allanite and epidote (10%), detrital feldspar (2%) and albite (5%) with accessory monazite, apatite, titanite and zircon (Supplementary Data: Electronic Appendix 1, Fig. S4.1). Allanite and mica compositions and allanite geochronology for one of the Scalaro quartzites (sample bva0824, No. 4, Table 2) have previously been reported by Rubatto *et al.* (2011). Here we report a more complete dataset for the same sample and compare it with the other Scalaro samples.

In most of the samples, two microscopic foliations were observed. Both are marked by white micas showing three compositions (Fig. 5c–e), as previously reported by Rubatto *et al.* (2011). Texturally older phengite cores (Ph-I: 3·35–3·48 a.p.f.u., pre-S_3 foliation) are surrounded by low-Si phengite (Ph-II: 3·20–3·25 a.p.f.u.), which are identical in composition to the white mica cores in S_3. The latter are, in turn, surrounded by high-Si phengite rims (Ph-III: 3·25–3·35 a.p.f.u., syn-S_3 foliation). Relict Ph-I is occasionally found in the cores of mica flakes aligned along S_3 (Fig. 5c and d). In some of the studied quartzites only the second and third generation of micas are preserved (Fig. 5f).

All quartzites contain abundant euhedral to subhedral grains of allanite (50–200 µm, 20–30 grains per thin section). Compositional zoning is common in these allanites (Supplementary Data: Electronic Appendix 1, Figs S4.2 and S4.3; see also Rubatto *et al.*, 2011). They show concentric growth zones with total REE contents normally decreasing from core (Aln core: REE + Y = 0·5–0·44 a.p.f.u.) to rim (Aln rim: REE + Y = 0·3–0·24 a.p.f.u.). Allanite is then rimmed and locally partially replaced by epidote (REE + Y < 0·05 a.p.f.u.).

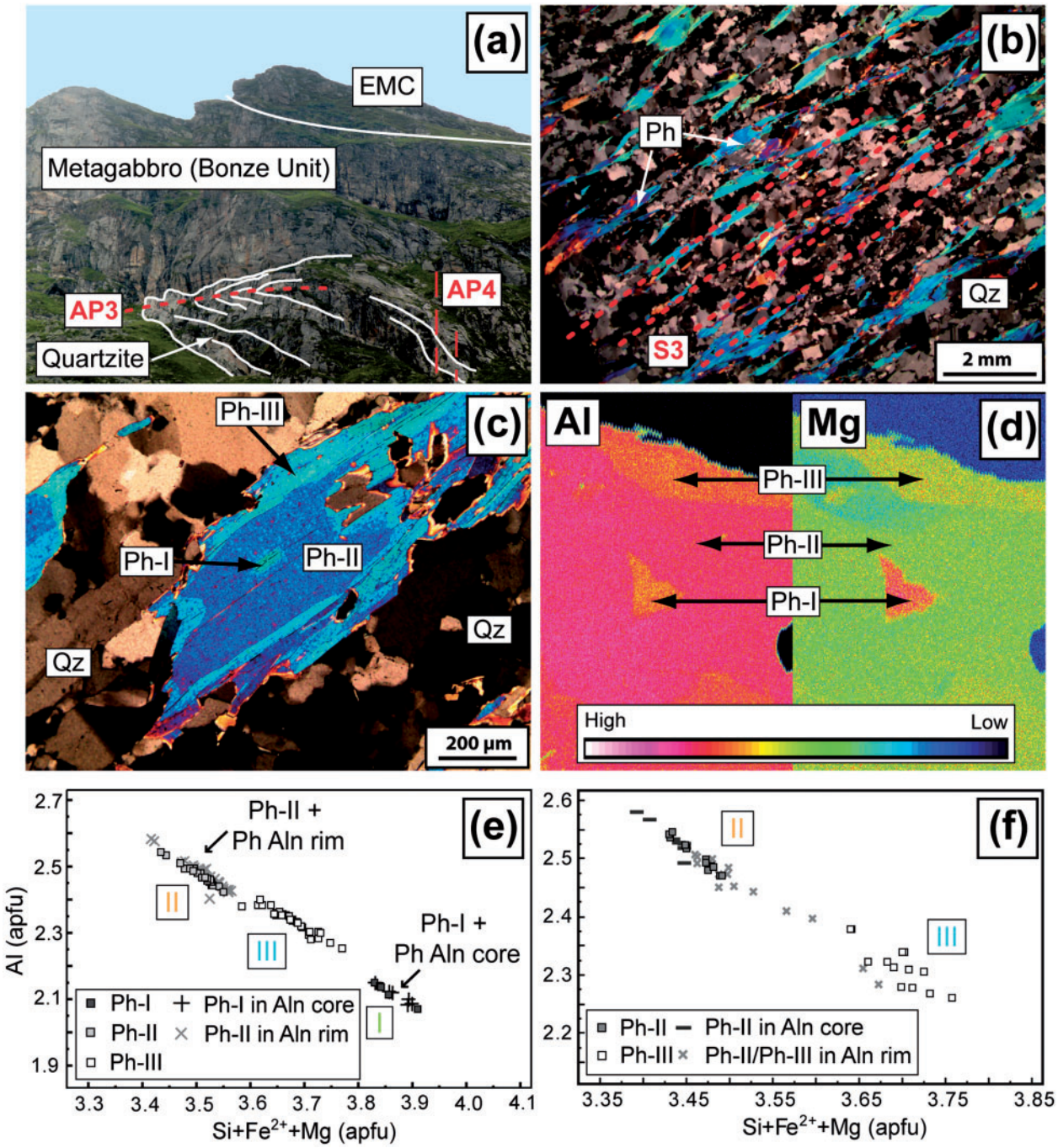

Fig. 5. Phengite-rich quartzite, Scalaro Unit. (a) Large-scale D_3 folds within impure quartzites (Scalaro Unit). S_3 axial planar foliation is re-folded by large-scale D_4 open folds with vertical axial planes. Quartzites are in tectonic contact with metagabbros (Bonze Unit). AP, trace of axial plane (AP3–AP4). (b) Microstructure of impure quartzite. S_3 foliation (axial planar foliation of D_3 folds) marked by phengite (Ph) in a quartz-rich matrix. Crossed-polarized light. (c) Photomicrograph showing different generations of mica and their textural relationship. Mica aligned parallel to S_3 foliation showing Ph-I relict cores. Crossed-polarized light. (d) Al and Mg distribution maps in mica flakes aligned along S_3. The higher Mg and Al contents in Ph-I and Ph-III according to the celadonite substitution between muscovite and phengite should be noted. (e) Composition of micas in sample No. 4 and micas included in allanite cores and rims. Micas in allanite cores correspond to the Ph-I composition; the compositions of micas included in allanite rims are indistinguishable from Ph-II. (f) Mica compositions in sample No. 5. No relics of Ph-I were preserved in this sample. Micas marking the S_3 foliation have Ph-II compositions in the cores and Ph-III in the rims. Micas included in allanite cores have Ph-II compositions; micas included in allanite rims are characterized by higher Si content (Ph-II and Ph-III composition).

Allanite cores and rims contain phengite inclusions. These were analyzed by electron microscope to compare their composition with that of mica marking the S_3 foliation. Abundant mica inclusions in the allanite cores (e.g. No. 4, Fig. 5e) are identical in composition to the texturally oldest phengite preserved in the sample (Ph-I). Allanite rims contain inclusions of mica, the composition of which is indistinguishable from Ph-II [see also Rubatto *et al.* (2011)]. In other samples (e.g. No. 5, Fig. 5f) allanite cores include Ph-II mica, whereas in the rims minute mica inclusions with a higher Si content (Ph-II–Ph-III) were observed.

PRESSURE–TEMPERATURE CONSTRAINTS

Druer tectono-metamorphic slice

The assemblage chloritoid–kyanite–garnet has been shown to be a key HP paragenesis that is stable over a restricted range of P–T conditions in the eclogite facies (e.g. Smye *et al.*, 2010). A model for the HP assemblage chloritoid–kyanite–garnet was calculated using the Gibbs free energy minimization algorithm Theriak/Domino (de Capitani & Brown, 1987; de Capitani & Petrakakis, 2010) and the thermodynamic database of Berman (1988) including more recent additions (see Supplementary Data: Electronic Appendix 1). The P–T diagram for the studied mica schist constrains the Grt + Cld + Ky + Ph + Pg + Qz assemblage in the range of 530–570°C and 1·5–2·4 GPa (Fig. 6). Further constraints can be obtained from phengite, garnet and chloritoid compositional isopleths. Comparison of the modelled isopleths of X_{Mg} (Cld), the Si contents in phengite, X_{Grs} (Grt) and X_{Alm} (Grt) with the mineral compositions determined in the samples allow the determination of the P–T conditions of the HP peak stage (where allanite is interpreted to be a stable phase) at 540–550°C and 1·9–2·0 GPa (Fig. 6).

Titanium-in-zircon thermometry was applied to constrain the conditions of zircon growth. The calibration of Watson *et al.* (2006) was applied with $a_{TiO2}=1$ and $a_{SiO2}=1$ for metapelitic rocks (Ghent & Stout, 1984), assuming rutile as the Ti-buffering phase as observed in thin section. The concentration of Ti in rim-I is in the range of 1·1–2·5 ppm; rim-II has lower concentrations, close to the detection limit (<0·7 ppm). These values indicate temperatures of 570–630°C for the first rim and $T<550$°C for the outermost metamorphic rim (Supplementary Data: Electronic Appendix 1, Fig. S1.4).

According to Zucali *et al.* (2002) and our own microscopic observations, chlorite is stable in syn-D_5 assemblages. It partially replaces garnet and forms from allanite breakdown. Chlorite thermometry was applied to better constrain the metamorphic conditions of the D_5 stage. Chlorite has an interesting potential for thermometric estimates because it displays a wide range of chemical compositions that reflect its physicochemical conditions of formation. Chlorite formed during the D_5 stage in the matrix and from allanite breakdown. Two thermometers were used: one proposed by Cathelineau (1988) on the basis of chlorite composition, and the software ChlMicaEqui (a MATLAB GUI-based program), which is based on the assemblage chlorite + quartz + water proposed by Vidal *et al.* (2001, 2005, 2006). With either method temperatures obtained on chlorite are below 380°C (Supplementary Data: Electronic Appendix 1, Fig. S1.7). The Cathelineau (1988) thermometer gave T in the range 330–380°C, whereas Vidal's method gave lower temperatures (300–355°C) with estimates of $X\mathrm{Fe}^{3+}$ ranging between 0·13 and 0·20 [using stoichiometric criteria given by Vidal *et al.* (2005, 2006)]. The obtained temperatures agree with those proposed by Zucali *et al.* (2002) for the D_5 stage.

Fondo tectono-metamorphic slice

Polymetamorphic metapelite (No. 2, Bonze Unit)

Equilibrium assemblage diagrams for the HP assemblage (M_1: jadeite + garnet + phengite) were produced using the Theriak/Domino software and the thermodynamic database of Berman (1988) including later additions (Supplementary Data: Electronic Appendix 1). To assess the importance of chemical fractionation as a result of garnet growth (e.g. Konrad-Schmolke *et al.*, 2011), the method described by Marmo *et al.* (2002) was applied for the calculated pseudosection. Applying this method shows that in sample bva0926 the Alpine garnets (mantle + rim) are not zoned enough to cause a significant fractionation of the bulk during their growth. To calculate the equilibrium composition during the growth of the Alpine garnet, the pre-Alpine garnet core was subtracted from the bulk-rock composition. The P–T assemblage diagram for the studied paraschist is shown in Fig. 7. It constrains the Grt + Wm (Ph) + Cpx + Ep + Rt + Qz assemblage in the range of 450–700°C and 1·4–2·2 GPa. Compositional isopleths of phengite (Si), garnet X_{Grs} and X_{Alm} and clinopyroxene X_{Jd} constrain the P–T conditions of the HP (M_1) peak stage at 520–560°C and 1·7–1·8 GPa (Fig. 7).

Metagabbro (No. 3, Bonze Unit)

Because most of these samples show disequilibrium textures that resulted from successive structural and metamorphic overprints, thermobarometry was applied only to mineral pairs in mutual contact with clear and sharp grain boundaries for the HP (M_1) assemblage. Several thermobarometers were applied to syn-D_1 mineral pairs. Temperatures were estimated by applying Mg–Fe exchange thermometers for coexisting garnet-clinopyroxene (Ellis & Green, 1979; Powell, 1985) and garnet–phengite (Green & Hellman, 1982) geothermometers. Pressures were estimated from the garnet–omphacite–phengite geobarometer (Waters & Martin, 1993). For the HP assemblage $T\sim530$°C (± 50°C)

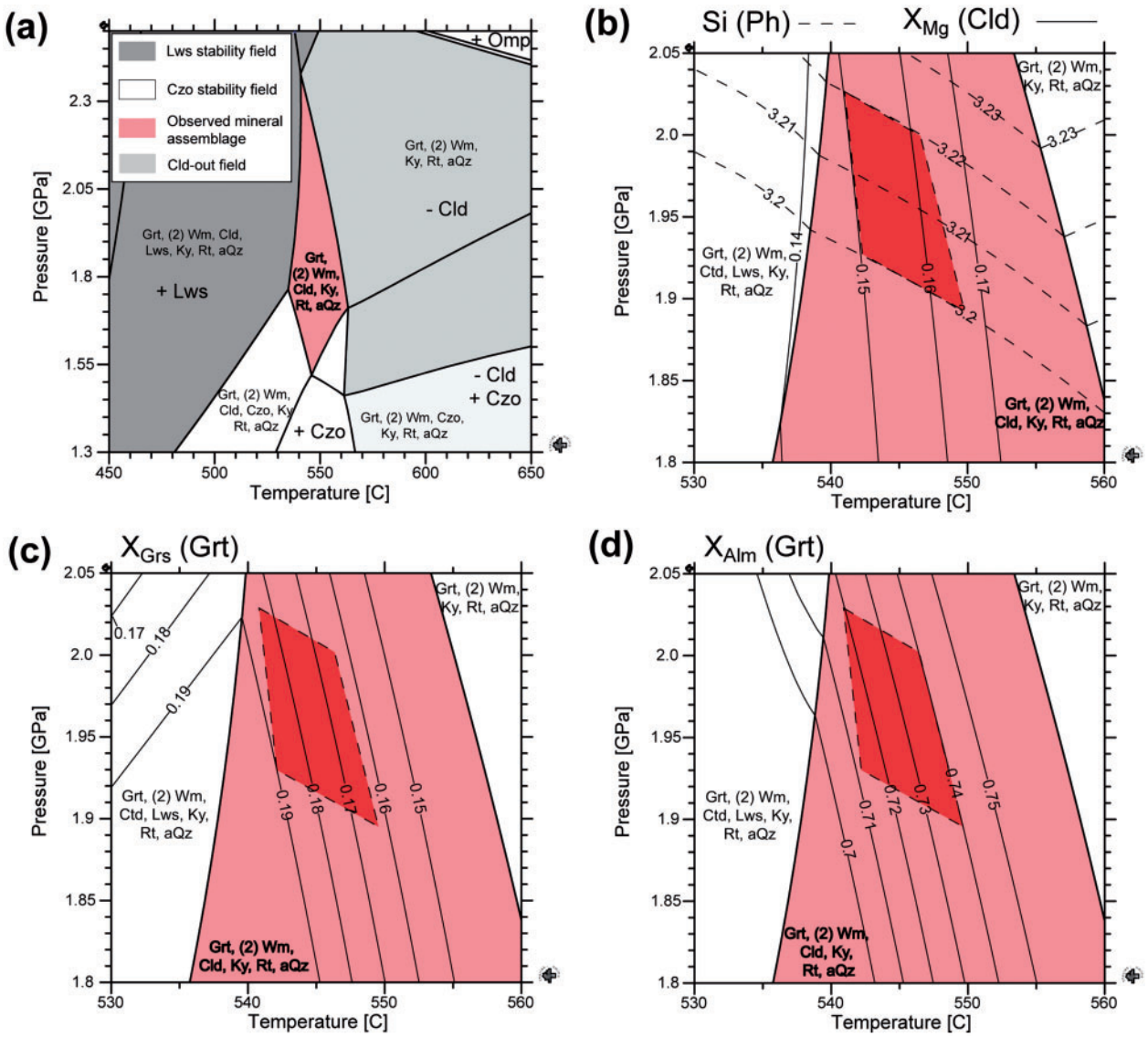

Fig. 6. Polymetamorphic metapelite, EMC. (a) P–T section showing the equilibrium phase relations for the observed mineral assemblage. The light red area marks the stability field of the HP mineral assemblage. Bulk composition (in moles): SiO_2 76·29, Al_2O_3 17·12, FeO 2·40, MnO 0·12, MgO 0·31, CaO 0·37, Na_2O 1·68, K_2O 1·59, TiO_2 0·15. Hematite–magnetite buffer included to take into account the excess of iron in the whole-rock composition; H_2O in excess. (b–d) Compositional isopleths: Si in phengite (Ph), X_{Mg} in chloritoid (Cld), X_{Grs} and X_{Alm} in garnet (Grt). Dark red field: nominal error box reflects uncertainties in microprobe compositions. Bulk-rock compositions were determined by XRF analysis and, for comparison, were estimated based on modal proportions (vol. %) and analyzed composition of the minerals. Wm, white mica component of Theriak/Domino.

and $P \sim 1{\cdot}7$ GPa ($\pm$ 0·1 GPa) were obtained. Equilibration temperatures about 30°C lower result from the calibration of Powell (1985).

Equilibrium assemblage diagrams for the MP assemblage (syn-S_2) were computed using the Theriak/Domino software (de Capitani & Petrakakis, 2010) and the thermodynamic database of Berman (1988) including recent additions for amphiboles (Supplementary Data: Electronic Appendix 1). The P–T diagram for the studied HP-assemblage constrains the Glc + Czo + Chl + Rt field in the range of 370–530°C and 0·8–1·55 GPa (Supplementary Data: Electronic Appendix 1, Fig. S3.7).

Darbellay (2009) studied the HG-zoisites from Cima Bonze in detail and found that the miscibility gap between the two zoisites ($X_{Ep} = 0{\cdot}1$ and $X_{Ep} = 0{\cdot}15$) corresponds to an equilibrium at 550 ± 50°C and 1·4–2·0 GPa [based on Gottschalk (2004)]. Although they described the zoisite as part of the HP assemblage, in the present study zoisite is interpreted to postdate the S_2 foliation on the basis of microtextural evidence.

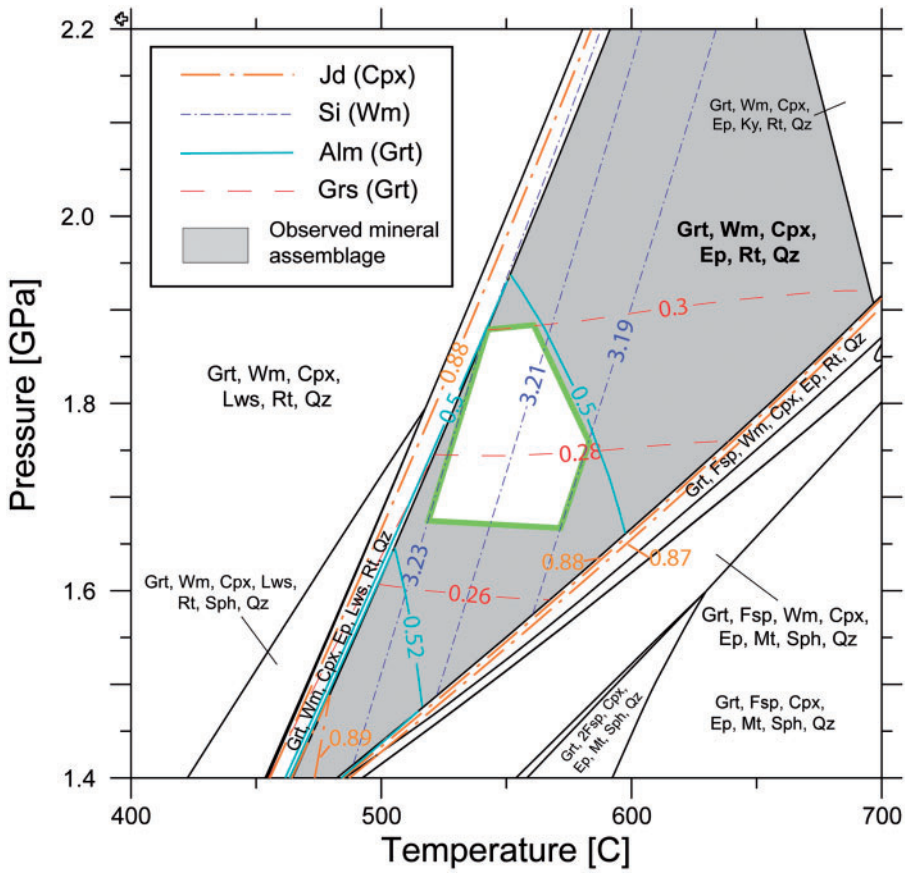

Fig. 7. Polycyclic metapelites, Bonze Unit. *P–T* equilibrium assemblage diagram calculated for SiO_2 64·90, Al_2O_3 16·30, FeO 1·88, MnO 0·03, MgO 0·28, CaO 2·40, Na_2O 13·92, K_2O 0·61, TiO_2 0·03 (in moles). Hematite–magnetite buffer included to take into account the Fe excess in the whole-rock composition; H_2O in excess. Compositional isopleths (Si in white mica (Wm), X_{Grs} and X_{Alm} in garnet and X_{Jd} in clinopyroxene) used to constrain the *P–T* conditions for the HP assemblage. The polygon reflects uncertainties in the microprobe compositions of the minerals and constrains the *P–T* conditions at which the HP assemblage developed. Bulk composition calculated from whole-rock XRF analysis.

The geothermobarometer of Okamoto & Toriumi (2004) was used to estimate the conditions of late actinolite crystallization. This thermobarometer permits the determination of *P–T* conditions for the stability of amphibole coexisting with Ep + Chl + Ab + Qz. This is particularly useful for mafic metamorphic rocks, for which the stability of the Act + Chl + Ep + Pl + Qz assemblage spans a wide range of *P–T*. Estimates were carried out on representative compositions from samples collected east of Colle Bonze and close to Cima Bonze. These data indicate 0·4–0·5 GPa and 390–430°C for Act-I and 0·15–0·25 GPa and 320–360°C for Act-II.

GEOCHRONOLOGY

Geochronological data (LA-ICP-MS, LA-MC-ICP-MS and SHRIMP) are summarized in Supplementary Data: Electronic Appendix 4. The age data are discussed below in some detail for samples from each tectono-metamorphic slice.

Druer tectono-metamorphic slice

In the chloritoid–kyanite–garnet mica schists (bva0840, No. 1, Table 2), allanite grains show homogeneous and occasionally patchy zoning, with relatively homogeneous Th/U values in the range of 5–15. Allanite contains 600–1500 ppm Th (LA-ICP-MS data) and a high proportion of initial Pb ($^{208}Pb_c = 60–80\%$ of the total ^{208}Pb measured), thus making the age calculation and the initial Pb correction strongly dependent on the common Pb composition chosen. The initial Pb corrections rely on assumed common Pb compositions (Stacey & Kramers, 1975) or upon U–Pb regressions. In the present case, the regression of the analyses in a Tera–Wasserburg diagram yields an initial $^{207}Pb/^{206}Pb$ of 0·8417 ± 0·014, which corresponds to that predicted by Stacey & Kramers (1975) at ~85 Ma. Additionally, we measured Pb isotope compositions by LA-MC-ICP-MS in minerals that are petrologically associated with allanite (mostly pyrite and white mica) to test the accuracy of the regressed composition (Supplementary Data: Electronic Appendix 1). The measured values are

within error of the model Pb composition of Stacey & Kramers (1975). This confirms that the assumption for the studied samples of initial Pb to be dominantly model common Pb is robust. The average $^{232}Th/^{208}Pb$ age obtained using the chosen common Pb composition is 85·8 ± 1·7 Ma (Fig. 8a). The constructed Th–Pb isochron for the same crystals (Fig. 8b) confirms the average age calculated (84·9 ± 2·1 Ma, MSWD = 2·3).

Zircon SHRIMP analyses were focused on the rims. Thirteen rim-I analyses define a cluster with a mean concordia age of 73·7 ± 0·8 Ma (Fig. 8c and d). Two analyses were not included because they returned significantly older dates and probably reflect mixing with the cores. The age of rim-II is not well constrained as $^{206}Pb/^{238}U$ dates scatter between 70 and 60 Ma (Fig. 8c and d).

Fondo tectono-metamorphic slice

Polymetamorphic metapelite (No. 2, Bonze Unit)

Zircons have inherited cores overgrown by three rims (Fig. 9). The analyses of the cores yielded two age groups, both characterized by high Th/U (0·4–0·6). The first group yields a mean concordia age of 510 ± 4·5 Ma (MSWD = 1·3) and the second one of 487 ± 4·5 Ma (MSWD = 0·75, Supplementary Data: Electronic Appendix 1, Fig. S2.9). The two groups of zircons are indistinguishable in terms of their trace element compositions (Supplementary Data: Electronic Appendix 1, Fig. S2.8). Cores are enriched in HREE at 10^3 times chondrite with a strong negative Eu anomaly (Eu_N/Eu^*_N 0·15).

The first rims (rim-I) overgrowing the Cambrian cores are characterized by low CL emission with high U contents. The three analyses that could be performed on these thin rims define a concordia age of 354 ± 18 Ma (Supplementary Data: Electronic Appendix 1, Fig. S2.9).

Zircon rim-II contains abundant HP inclusions (e.g. jadeite, phengite, rutile). Six analyses of these rims yield an average $^{206}Pb/^{238}U$ age of 74·6 ± 2·1 Ma (Fig. 9). The analyses carried out on the most external domains (rim-III) yield mixed dates ranging between 70 and 63 Ma (Fig. 9).

In an attempt to link zircon growth with a specific tectono-metamorphic stage, REE partitioning values were calculated for the different generations of zircon and garnet. Partitioning between zircon rim-II and Grt mantles for the HREE is within one order of magnitude of what has been reported for HP rocks by Rubatto & Hermann (2003, 2007), suggesting that the garnet mantle probably grew with the generation of zircon including jadeite (Supplementary Data: Electronic Appendix 1, Fig. S2.10). There is, however, disagreement between our data and previously reported values for the MREE and this is may be due to other MREE phases being present in our samples, or lack of preservation in the garnet or zircon record.

Monometamorphic phengite-rich quartzites (Nos 4–8, Scalaro Unit)

A single dating method may not be sufficient to unravel the complex *P–T*–time evolution of a poly-deformed rock, as shown for the polycyclic samples. To complement and supplement the obtained data, particular emphasis was placed on impure quartzites as these contain abundant allanite crystals with concentric growth zones in a commonly sub-pelitic matrix. The different generations of allanite were dated by SHRIMP analysis in five samples (Table 2) using the Th–Pb system. The epidote rims were always too rich in common Pb to be dated.

Allanite ages for sample No. 4 (Table 2) were presented by Rubatto *et al.* (2011; their sample B24). Allanite cores yield consistent $^{208}Pb/^{232}Th$ ages with an average of 75·6 ± 1·5 Ma (Fig. 10a). Allanite cores and rims contain minute phengite inclusions. Mica inclusions in allanite cores are identical in composition to the texturally oldest phengite preserved in the sample (Ph-I, Fig. 5e). The REE-poor allanite rim is significantly younger, at 69·4 ± 1·4 Ma (Fig. 10b), and contains inclusions of Ph-II.

In sample No. 5 (Table 2) allanite cores yield a $^{208}Pb/^{232}Th$ average age of 68·1 ± 1·8 Ma (Fig. 10c) and again consistently younger ages in the rim (62·8 ± 1·3 Ma, Fig. 10d). As in sample No. 4, mica inclusions in allanite are common. In allanite cores, micas have Si contents similar to Ph-II, whereas small crystals included in allanite rims are characterized by higher Si contents (3·20–3·30 a.p.f.u.; see Fig. 5f).

In sample No. 6 (Table 2) only allanite cores were dated (72·1 ± 1·4 Ma) because the rims have high common lead contents ($^{208}Pb_c > 85\%$ of the total ^{208}Pb). In sample No. 7 (Table 2) allanite cores yielded a $^{208}Pb/^{232}Th$ age of 68·1 ± 1·4 Ma, whereas the rims gave an age of 60·1 ± 1·2 Ma. The measured allanite cores in sample No. 8 (Table 2) yield an age of 74·1 ± 1·5 Ma, whereas the rims are systematically younger at 68·2 ± 1·9 Ma (Supplementary Data: Electronic Appendix 1). In these samples, allanite contains only quartz inclusions.

The three allanite populations documented in five samples (Fig. 10e) are thus indicative of a cycle from high pressure (~75 Ma, inclusions of Ph-I) to medium pressure (~68 Ma, inclusions of Ph-II), followed by another HP stage at 65–62 Ma. This last stage is probably represented by the texturally late high-pressure foliation (S_3 marked by Ph-III), which is well developed in these samples.

DISCUSSION

Pressure and temperature are regularly determined by chemical equilibria between different rock-forming minerals whereas time is determined by radioactive decay of elements such as U–Th to Pb in accessory phases such as allanite, monazite and zircon. These chronometers are arguably the most important for inferring tectonic processes

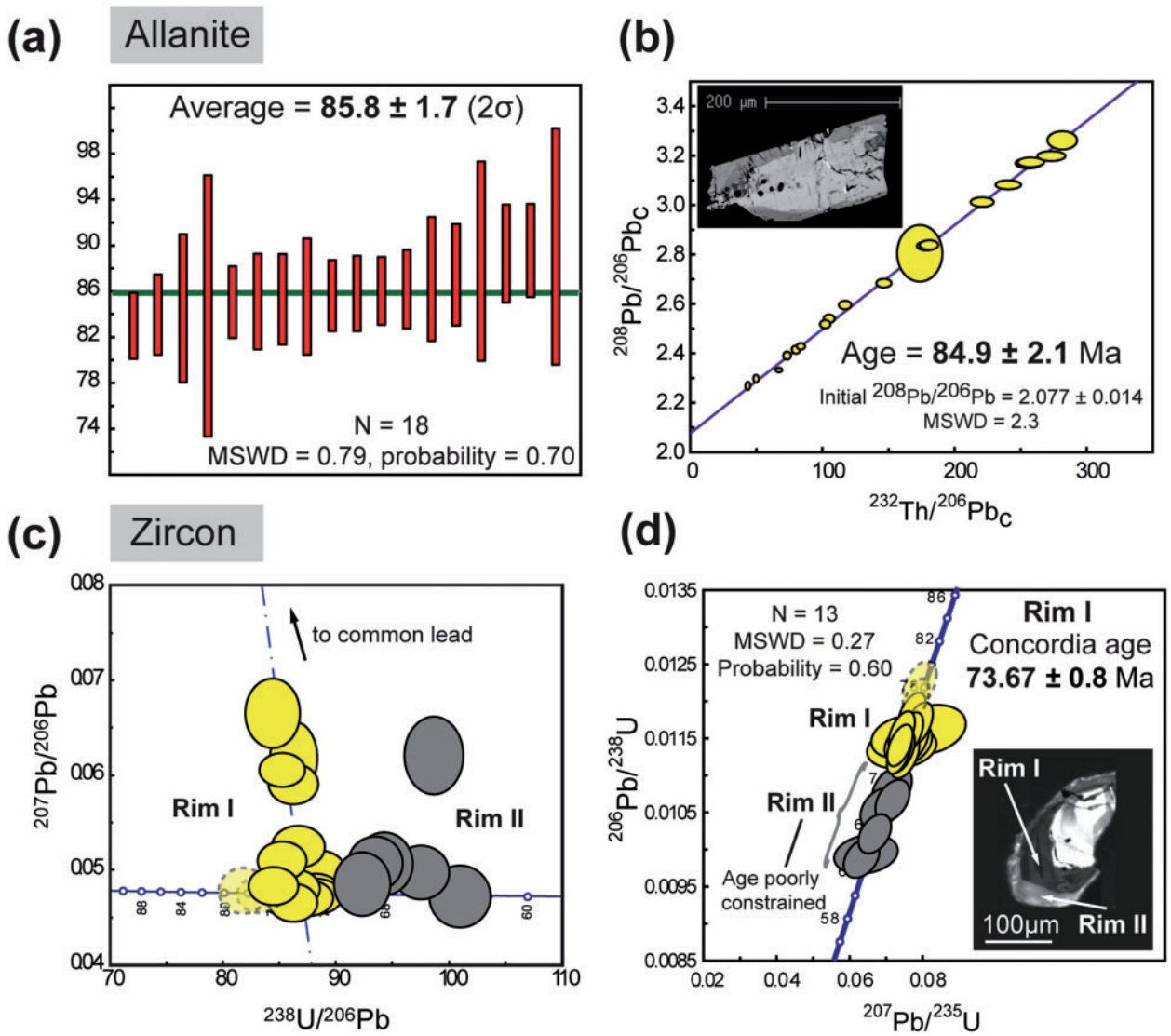

Fig. 8. Polymetamorphic metapelite, EMC. (a) Allanite average $^{232}Th/^{208}Pb$ age. Box heights are 2σ. (b) Th–Pb isochron for allanite. (c) Tera–Wasserburg plot for SHRIMP zircon U–Pb analyses. (d) Concordia plot for zircon rims. The transparent ellipses are data points excluded from the age calculation. Rim-II shows age scatter that can be related to partial mixing with older domains (small size of rim-II: 10–15 μm). Data-point error ellipses are 2σ.

(e.g. Gabudianu Radulescu *et al.*, 2009; Warren *et al.*, 2011); however, complexities in the growth and dissolution behavior of these minerals mean that the interpretation of their ages in relation to the evolution of their host rock-forming minerals is still in its infancy. In the following sections we integrate textural observations with petrological, microchemical and age data to reconstruct the complex *P–T–*time history of the two tectono-metamorphic slices.

Evolution of the Druer tectono-metamorphic slice

In the Druer samples, the allanite cores show microstructural equilibrium with all of the minerals defining the peak assemblage. Moreover, allanite exhibits no Eu anomaly, which, as commonly interpreted for zircon (Rubatto, 2002), suggests that allanite grew outside the plagioclase stability field (>1·1–1·2 GPa according to equilibrium assemblage diagrams; Fig. 11). Allanite is therefore considered to record the age of HP metamorphism. The widespread occurrence of clinozoisite coronae (overgrowing the S_2 foliation) on allanite indicates that they grew most probably during the D_4 stage (Fig. 11). In the most retrogressed samples, breakdown of allanite + clinozoisite is common; both phases are replaced by fine-grained chlorite + synchysite + clay minerals ± apatite (Fig. 11). In some reaction domains, relics of allanite are still observed (Fig. 11); in other domains, allanite + clinozoisite are completely pseudomorphed (Fig. 11).

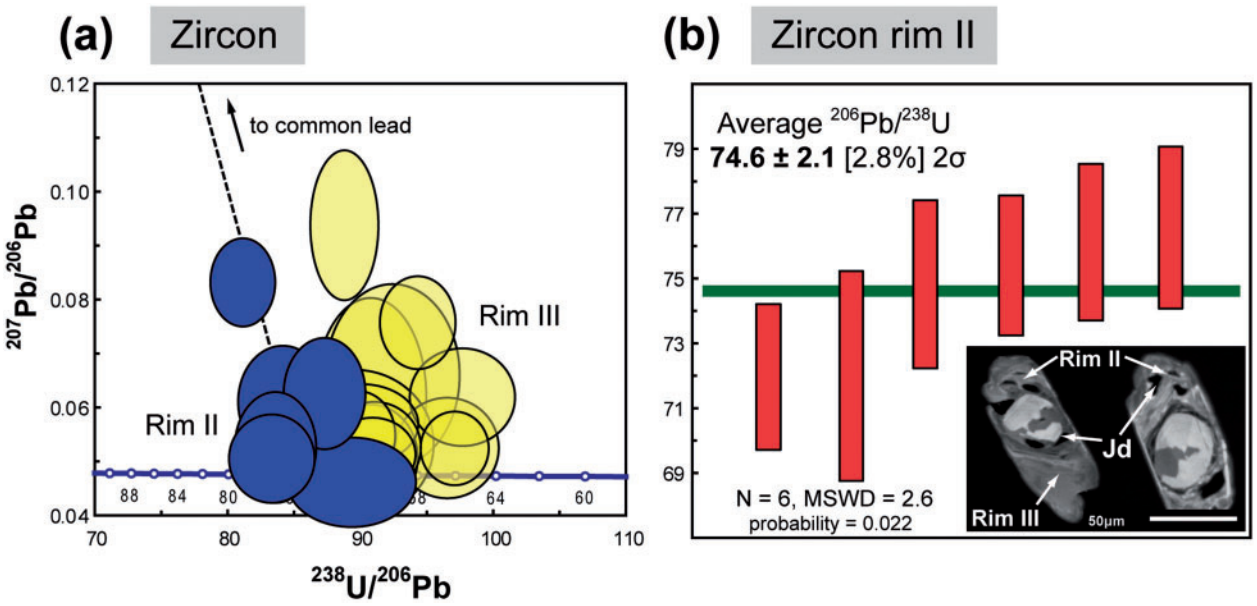

Fig. 9. Polycyclic metapelite, Bonze Unit. Tera–Wasserburg plot for SHRIMP zircon U–Pb analyses and CL image of the analyzed zircons. Data-point error ellipses are 2σ.

Zircon rims are systematically younger than allanite. Their zoning and chemical composition (low Th/U) and Ti-in-zircon temperatures indicate that they also formed during metamorphism. Both rims are characterized by flat HREE patterns, suggesting that garnet was present in the assemblage at the time of zircon formation; the lack of an Eu anomaly suggests that plagioclase was not stable (Rubatto, 2002) and thus that pressure was >1·2 GPa. According to the *P–T* path of Fig. 11, these constraints indicate that zircon also formed at HP conditions.

In summary, the main metamorphic stages (Fig. 11) documented in the Druer slice are as follows.

- *Dr-HP1 stage*. The HP peak-mineral assemblage (chloritoid + kyanite + garnet + phengite + paragonite + rutile) was stable at 540–550°C and 1·9–2·0 GPa. Allanite is in equilibrium with this prograde assemblage and constrains the age of this HP stage to about 85 Ma.
- *Dr-HP2 stage*. A first generation of metamorphic zircon grew during the early stage of exhumation (at ~74 Ma); growth occurred together with garnet, above the pressure of feldspar stability. Ti-in-zircon thermometry indicates temperatures of 570–630°C; that is, heating during decompression.
- *Dr-MP stage*. A second generation of metamorphic zircon growth occurred between 70 and 60 Ma, probably jointly with the formation of clinozoisite at temperatures below 550°C, but still at pressures above the stability field of plagioclase (Fig. 11).
- *Dr-LP stage*. During late stages of exhumation (<30 Ma?) allanite + clinozoisite were replaced by chlorite and synchysite, at temperatures of 380–300°C (Fig. 11; Supplementary Data: Electronic Appendix 1, Figs S1.5–S1.7).

Evolution of the Fondo tectono-metamorphic slice

Samples from the Scalaro–Bonze Units (Fondo tectono-metamorphic slice) display several segments of an evolutionary path at high-pressure conditions. Impure and pure quartzites occur closely interbedded with albitic gneisses within the Scalaro Unit, making up continuous meter-thick horizons. From one outcrop sequence to the next, details of the tectono-stratigraphy often appear comparable at a small scale, although internal structural discontinuities are common (Venturini, 1995). The monometamorphic metasedimentary horizons accompany mafic rocks and associated metasediments, which display a pre-Mesozoic metamorphic imprint. These observations indicate that variable amounts of old basement material were tectonically juxtaposed to the Scalaro sediments, either at a rifting stage or during early convergence. In addition to locally preserved pre-Alpine relics, the polycyclic metasediments show synkinematic assemblages of an early Alpine low-*T* eclogite facies (M_1–D_1) and a subsequent blueschist facies (M_2–D_2) (Figs. 12a and b). Detailed constraints on the multi-stage Alpine evolution of the Scalaro and Bonze Units were derived by combining petrographic and microstructural evidence from the entire sample suite. Both units appear to have undergone the same Alpine *P–T–t* evolution, probably associated

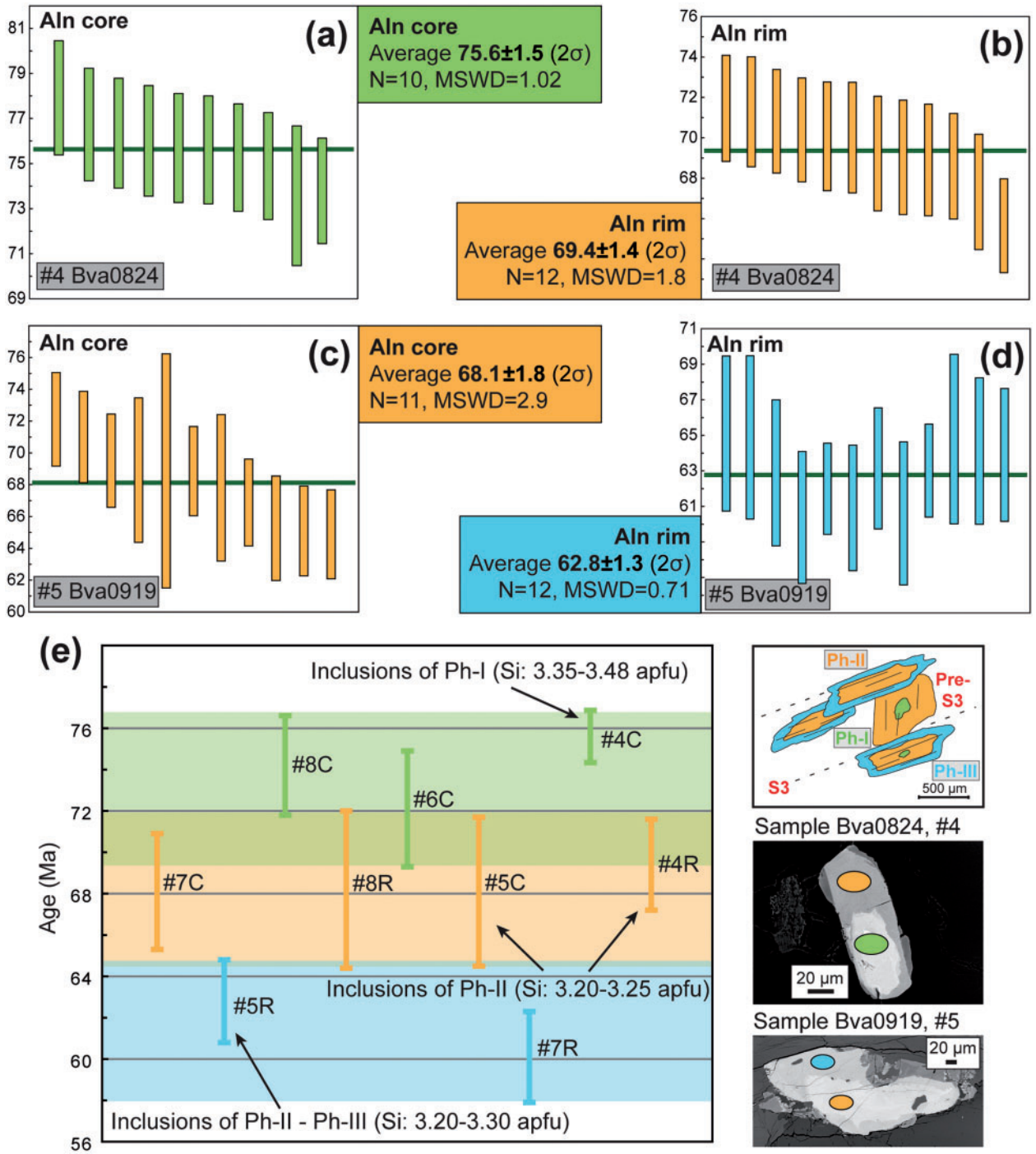

Fig. 10. Phengite-rich quartzites, Scalaro Unit. (a, b) Average $^{208}Pb/^{232}Th$ age for allanite core and rim in sample bva0824 (No. 4). Composition of micas included in both Aln core and rim is shown in Fig. 5e. (c, d) Average $^{208}Pb–^{232}Th$ age for allanite core and rim in sample bva0919 (No. 5). Compositions of micas included in Aln core and rim in this sample are shown in Fig. 5f. In (a–d) box heights are 2σ. (e) Summary of the three allanite age populations in five quartzite samples. Numbers at each age refer to the sample number in Table 1; C, core analysis; R, rim analysis. For samples No. 4 and No. 5 the Si contents of micas included in core and rim are indicated. On the right: sketch of mica generations: high-Si Ph-I (pre-S_3 foliation) is rimmed by low-Si Ph-II mica. Syn-S_3 high-Si Ph-III overgrows Ph-II. BSE images of allanite in samples Nos 4 and 5. Ellipses correspond to SHRIMP spots (25 µm); ellipse colors correspond to the age groups.

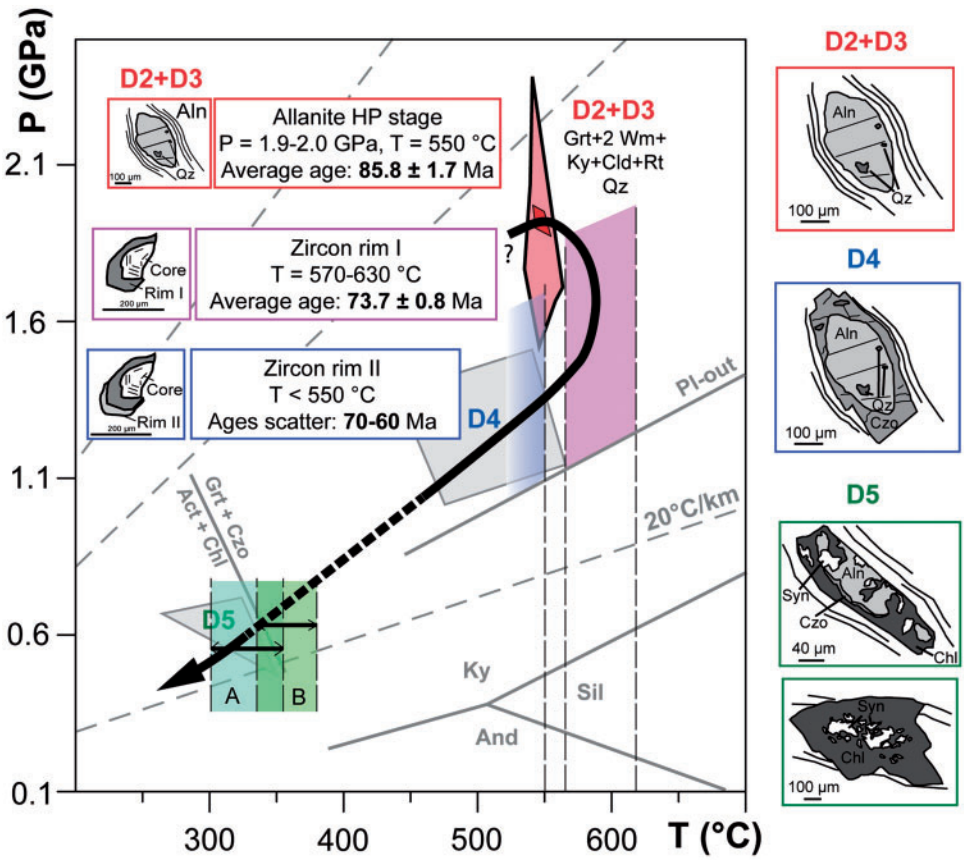

Fig. 11. *P–T–t* paths inferred from metapelites and metabasites from the Druer slice in the central Sesia Zone. Stages D_4 and D_5 are from Zucali *et al.* (2002). On the right: metamorphic sequence of accessory allanite.

with metasediments belonging to the EMC. Given their ductility and limited thickness (<400 m), the Scalaro metasediments are unlikely to represent a 'tectono-metamorphic slice' on their own. It is more plausible to view them as part of larger slice, together with their at present associated polymetamorphic rocks (i.e. the Bonze Unit) and the adjacent package(s) of basement [e.g. Intermediate Unit of Venturini (1995); see Fig. 1a]. Thus far it is uncertain when the Scalaro–Bonze slice was tectonically assembled. From our data, however, it is clear that it was tectonically juxtaposed against other such slices, reflecting the documented differences in their *P–T–t* paths.

Referring to Figs 12 and 13, the main stages in the formation of the Fondo slice (Fnd) were as follows.

- *Fnd-HP1 stage*. Temperatures of 500–550°C and pressures of 1·7 GPa were obtained for all of the mafic samples (metagabbros) examined; these match the most reliable *P–T* estimates given for the peak conditions in the associated polymetamorphic metasediments (*T* 520–560°C, *P* 1·7–1·8 GPa). Jadeite inclusions in Alpine metamorphic zircon (rim-II, low Th/U, sample No. 2) suggest that ~75 Ma (Fig. 13) is the age of the first high-pressure stage (HP1). This is also supported by trace element partitioning between zircon rim-II and garnet mantles and inclusions of Ph-I (pre-S_3) in allanite cores (dated at ~74 Ma, Figs 12 and 13) in impure quartzites.
- *Fnd-MP stage*. Decompression was recorded at ~68 Ma (Fig. 13), both in basic rocks (S_2 Gln-foliation) and in impure quartzites (MP Ph-II in allanite dated at 68·1 ± 1·8 Ma). Pressure and temperature conditions could not be precisely constrained for this stage (Fig. 13 and Supplementary Data: Electronic Appendix 1, Fig. S3.7), but the drop evident in the Si contents of phengite (from ~3·45 a.p.f.u. at the HP1 stage to ~3·20 a.p.f.u. at the MP stage) is significant.
- *Fnd-HP2 stage*. Growth of hour-glass zoned zoisite occurred after the formation of the glaucophane–clinozoisite mylonitic foliation (S_2) at 550 ± 50°C and between 1·4 and 2·0 GPa. Similar conditions can be related to Si-rich phengite (Ph-III) in quartzite, where mica grew during S_3 deformation. Allanite ages from samples No. 5 and No. 7 (Fig. 13) restrict the HP2 stage to 65–60 Ma.

SHRIMP and LA-ICP-MS dating of both allanite and zircon yields an age gap of several million years between

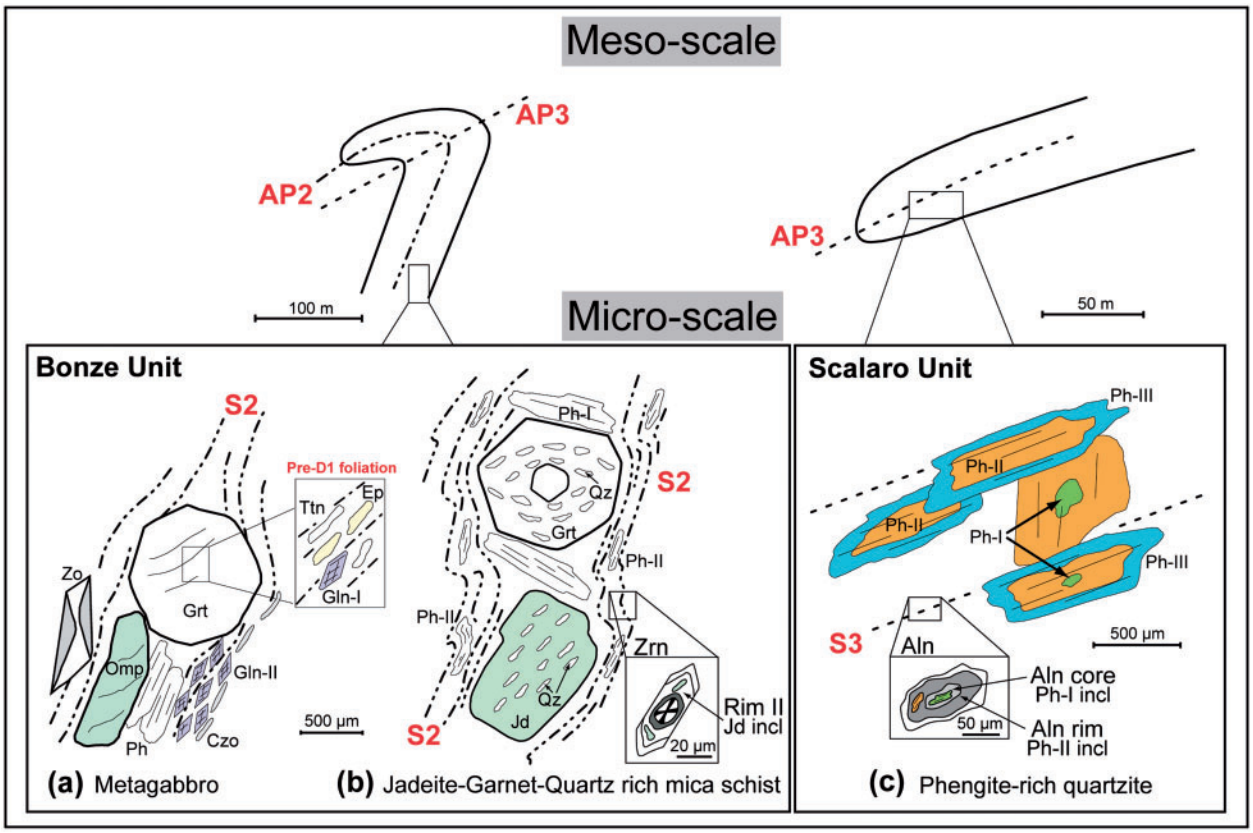

Fig. 12. Schematic sketches of meso- and microstructural relationships in basic rocks and poly- and monometamorphic metasediments of the Fondo tectono-metamorphic slice (Bonze and Scalaro units) inferred from microstructural analysis. HP1 stage assemblages preserved within metagabbro and Jd–Grt mica schist are wrapped by MP S_2 mylonitic foliation (axial planar foliation of D_2 folds). S_2 is refolded by D_3 folds with development of a new foliation (S_3) marked by HP2 phengite (Ph-III). HP1 zircons with inclusions of Jd were dated at ~75 Ma (b); this stage correspond to allanite core ages (~74 Ma) with inclusions of Ph-I (c).

two stages of the HP evolution, which has been attributed to tectonic cycling ('yo-yo subduction'), as described for similar rocks by Rubatto *et al.* (2011; Fig. 13). The alternative possibility that the pressure difference may largely reflect variations in tectonic overpressure (e.g. Mancktelow, 2008) does not appear very likely, as the various pressure stages have been documented in several samples, which were taken kilometers apart from lithologies that are rheologically weak. Whereas the enclosing basement rocks are at least in part stronger, and one might imagine that they acted as confining walls exerting pressure variations on the metasediments, the lateral extent of the outcrops makes it likely that such an enclosure would have been leaky; that is, unable to sustain substantial tectonic overpressure. For these reasons, the observed pressure variation is attributed mostly to tectonic cycling, requiring a vertical amplitude of 10–20 km (Fig. 13). The cycling rate for the Fondo slice (i.e. the rate of decompression followed by renewed subduction) is of the order of 2–3 mm a^{-1}, which is comparable with rates that have been proposed for several subduction complexes [Roda *et al.* (2010) and references therein] and significantly slower than the fast exhumation of other units within the Western Alps (e.g. Rubatto & Hermann, 2001).

INDEPENDENT EVOLUTION OF THE TECTONO-METAMORPHIC SLICES

The two tectono-metamorphic slices investigated belong to distinct portions of the Sesia Zone, the Scalaro–Bonze Units and the Eclogitic Micaschist Complex, which show different *P–T–t* evolution. This suggests that these two units may have been moving independently from one another within the same subduction channel. Within the polymetamorphic samples of the Druer slice, no pressure cycling has been recognized so far. These inferences are in line with earlier studies from the same area (e.g. Reinsch, 1979; Lardeaux *et al.*, 1982; Zucali *et al.*, 2002) and notably the detailed study of Zucali & Spalla (2011). Those researchers described the lawsonite-bearing rocks of the Ivozio Complex (northern Sesia Zone) as a

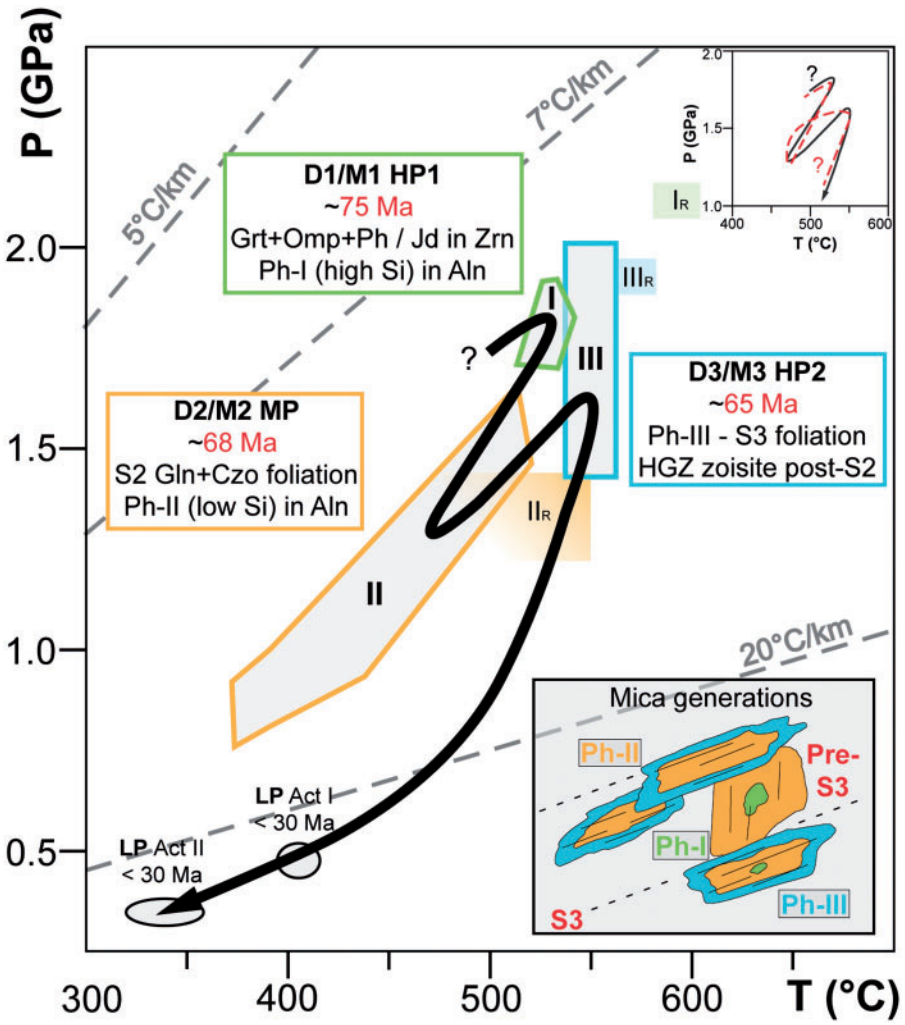

Fig. 13. *P–T–t* path inferred from metapelites, metabasites, and impure quartzites for the Fondo slice in the central Sesia Zone. Stages I_R, II_R, III_R have been described by Rubatto *et al.* (2011).

tectono-metamorphic unit characterized by a clockwise *P–T* path (HP stage: $T > 600°C$ and $P > 2{\cdot}25$ GPa), documenting heating between the *P–T* peak conditions and the end of the decompression. In the southern Sesia Zone, in contrast to the northern Sesia Zone, retrograde growth of lawsonite indicates a counterclockwise path (Pognante, 1989; Spalla & Zulbati, 2003). Such peculiar *P–T–t* paths, which are different from those that we report for the Druer and Fondo slices, indicate that the EMC actually consists of several tectono-metamorphic units (e.g. Spalla *et al.*, 2005). To define the size and shape of potentially coherent units (i.e. those with a uniform *P–T–t* evolution) it is important to link the details of the metamorphic evolution and the attendant small-scale structures within single samples and single outcrop sequences to the large-scale structural context and the deformation domains, such as those recognized by Zucali *et al.* (2002) and Babist *et al.* (2006).

As emphasized by Zucali & Spalla (2011), single slices, including parts of the EMC, followed their own *P–T–t* paths and may have been decoupled from other slices, owing to mechanical processes within the subduction channel. The independent motion of tectonic slices within that channel has been unambiguously demonstrated in the present case because the Fondo and the Druer slices underwent different *P–T* conditions at the same point in time (Fig. 14). An array of diverse *P–T* paths for subduction-related metamorphic complexes rather than a single *P–T* trajectory has been predicted by numerical models (e.g. Gerya *et al.*, 2002; Roda *et al.*, 2012). The present field-based study confirms that principle and sets some quantitative limits on the kinematics at eclogite-facies conditions. However, the detailed chronology needed to identify further potentially independent slices—for example, in the southwestern part of the Sesia Zone (e.g. Pognante, 1989)—is at present lacking.

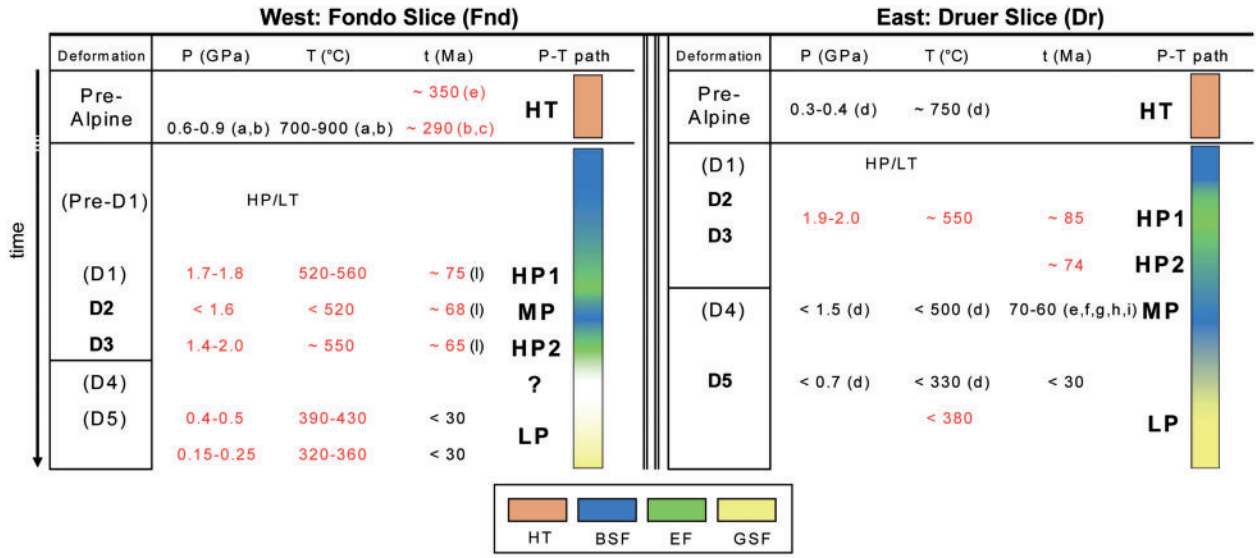

Fig. 14. Summary *P–T–t* results for the studied tectonometamorphic slices (Fondo and Druer slices). New data from this study are reported in red. Literature data (in black) are from (a) Lardeaux & Spalla (1991), (b) Rebay & Spalla (2001), (c) Bussy *et al.* (1998), (d) Zucali *et al.* (2002), (e) Rubatto *et al.* (1999), (f) Venturini (1995), (g) Inger *et al.* (1996), (h) Duchêne *et al.* (1997), (i) Ruffet *et al.* (1997), (l) Rubatto *et al.* (2011). For each slice the colored column indicates the metamorphic conditions at different deformation stages (HT, high temperature—amphibolite or granulite facies; BSF, blueschist facies; EF, eclogite facies; GSF, greenschist facies). It should be noted that the two slices have experienced different metamorphic conditions at the same time. Cima Bonze deformation stages are modified after Babist *et al.* (2006); Mombarone deformation stages are from Zucali *et al.* (2002).

In the present case, tectonic cycling has been so far documented only for the smaller Fondo slice (Fig. 13), and it is not clear if any of the larger slices were involved in 'yo-yo subduction'. The reconstructed evolution path of the Druer tectono-metamorphic slice lacks any evidence of an intermediate lower pressure stage between HP1 and HP2, and thus suggests that this slice underwent prolonged eclogite-facies metamorphism between 85 and 75 Ma (Fig. 11). Heating upon initial decompression implies a relatively slow start of the upward movement, slower in any case than the upward relaxation of the depressed isotherms.

The particular behaviour of the Fondo slice, involving pressure cycling, may be additionally related to the acute convergence angle proposed for the respective time interval (i.e. 75–68 Ma; Rubatto *et al.*, 2011). Under such geometric conditions, it is conceivable that some tectonic fragments went through phases of transpression and relative transtension in response to strain partitioning and changes in the rheology along the subduction interface.

According to the regional tectonic framework proposed by Babist *et al.* (2006), the two main basement nappes of the Sesia Zone were amalgamated with the trail of Scalaro metasediments sandwiched between them at HP conditions, prior to the complex exhumation history. Previous workers (Passchier *et al.*, 1981; Williams & Compagnoni, 1983; Inger *et al.*, 1996) asserted that the two main Sesia complexes (albeit delimited in different terms) had separate early metamorphic histories and were juxtaposed by thrusting after the peak of high-pressure metamorphism. Although the present study confirms independent movements, we conclude that the assembly of the Sesia terrane as a whole is considerably more complex. It cannot be simply described by the juxtaposition and evolution of just two main complexes because several slices (e.g. Fondo and Druer) were involved. Their size, geometry, and the contacts against adjacent slices have not yet been documented in detail, and published maps and field reports need to be complemented and re-evaluated. Investigating the *P–T–t* history of further samples may well add details on the movement of other slices and thus of the dynamics in deep portions of convergent margins. As the present study shows, it is critical to couple petrochronology with meso- and microstructural observations to integrate the data into the regional context.

At the present stage of understanding, we regard the Fondo and Druer slices as tectonic fragments that moved independently of each other, at least during the early stages of the evolution of the subduction channel in the central Sesia Zone. These fragments followed different *P–T* paths, under eclogite-facies conditions, up to their juxtaposition, which most probably occurred after the HP2 stage (age <65 Ma). Pressure–temperature diagrams for samples from the two slices indicate a coherent evolution in the subsequent exhumation history (Fig. 15).

It thus appears that the regional ages previously recognized for HP metamorphism in the Sesia Zone mostly

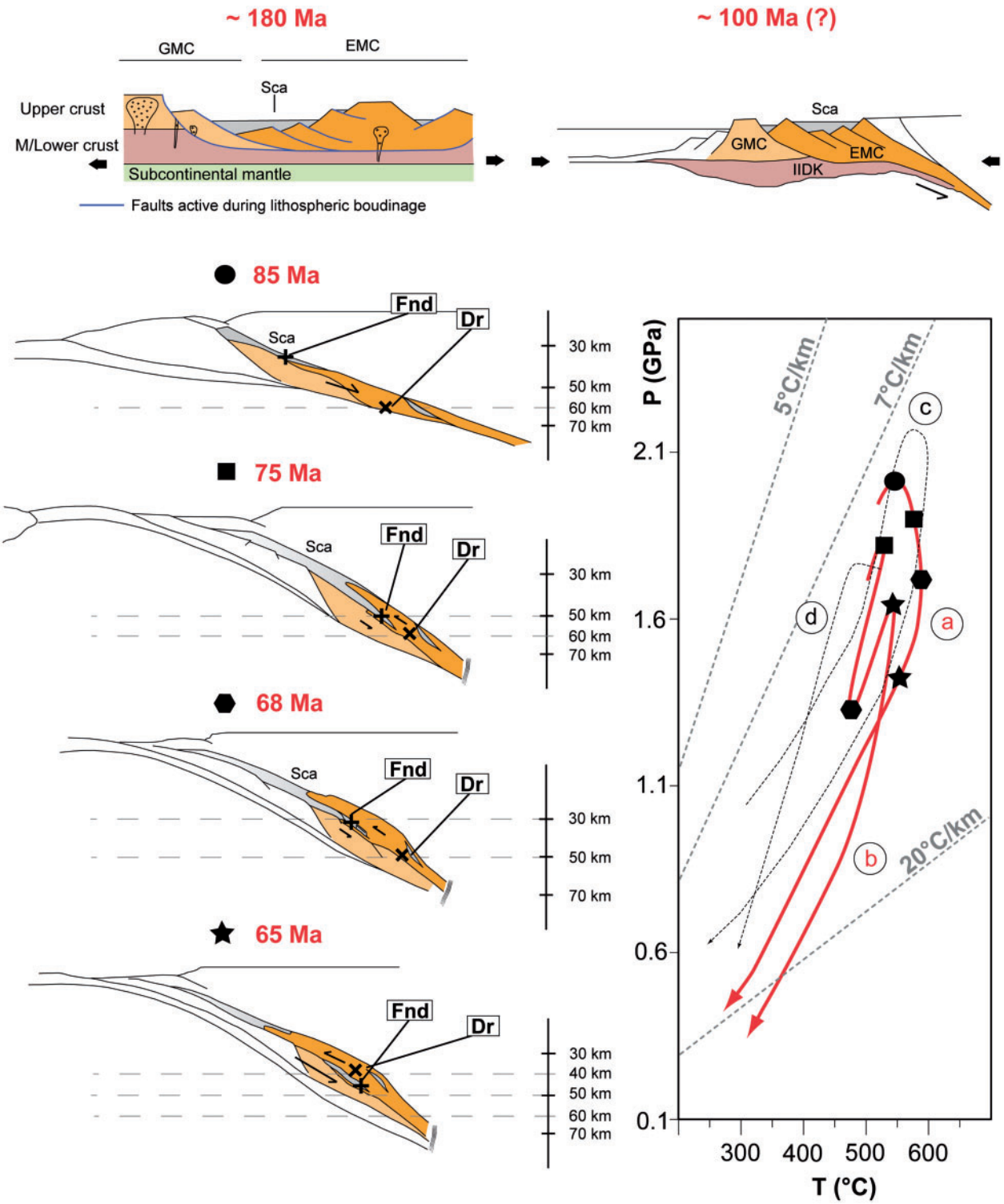

Fig. 15. Simplified tectonic model for subduction and exhumation of the Sesia Zone based on the new data presented in this work and *P–T* diagrams for the various tectonic slices recognized. (See text for explanation of stages.) In the *P–T* grid on the right, a and b are the *P–T* paths for the Druer (Dr) and Fondo (Fnd) slices respectively (symbols represent different age stages as shown in the model); c is the *P–T* evolution of the Ivozio Complex [modified after Zucali & Spalla (2011)]; *d* is the *P–T* evolution of the southern Sesia Zone [modified after Pognante (1989) and Spalla & Zulbati (2003)]. GMC, Gneiss Minuti Complex; EMC, Eclogitic Micaschist Complex; Sca, Scalaro Unit; IIDK, Second Dioritic–Kinzigitic Zone.

reflect this last stage (HP2; e.g. Duchêne *et al.*, 1997; Rubatto *et al.*, 1999). The distribution of earlier ages reported in the literature (from Middle to Late Cretaceous) may reflect the rather complex evolution of the Sesia Zone, which is now becoming better constrained. The current identification of independent units within this zone demands a re-evaluation of these ages, considered to record HP metamorphism, and of the array of potential problems in the dating techniques used.

An extensive discussion of earlier geochronological results is beyond the scope of the present study. However, it is remarkable that for monometamorphic quartz-rich marbles and impure quartzites (Scalaro Unit), Venturini (1995) reported $^{40}Ar/^{39}Ar$ ages scattering between 60 and 80 Ma. The multiple generations of white mica recognized in our samples from that area may help to explain the remarkable diversity of Ar–Ar age data reported by Venturini (1995). Our detailed petrochronological approach allows several steps of the HP evolution to be identified within the time span documented by Venturini (1995). The range of Ar–Ar ages (Venturini, 1995) for polymetamorphic samples remains, however, far larger, and problems of inheritance and excess argon are likely to have masked potentially discernible HP stages.

ASSEMBLY OF THE SESIA ZONE

To explain the diverse array of P–T–t paths observed within the central Sesia Zone (Druer and Fondo slices), we propose a new simplified tectonic model for the subduction, exhumation and assembly of the Sesia Zone as a whole (Fig. 15). The schematic illustration in Fig. 15 shows graphically the tectonic context and highlights some of the tectonic implications of the new data presented in this study.

The initial geometry in Jurassic time is adopted from previous studies (e.g. Babist *et al.*, 2006; Handy *et al.*, 2010). During extension (~180 Ma) listric faults broke up parts of the NW Adria margin, including segments of continental crust that were later incorporated in the two main Sesia units (i.e. the Eclogitic Micaschist Complex and the Gneiss Minuti Complex). It is possible that these segments were already separated at this rifting stage into subunits that later behaved as independent slices. In any case, intracontinental or marginal basin sediments (e.g. Scalaro Unit) were deposited between and on top of different tectonic slices.

Incipient subduction (compression stage) most probably started at 130–100 Ma and led to the HP stage at ~85 Ma in the Druer tectono-metamorphic slice (~60 km depth). At ~75 Ma the Druer slice was still at high pressure. Much of the associated deformation was probably accommodated at the boundary between the two main complexes (GMC and EMC). At ~75 Ma, while the Druer slice was being slowly exhumed, the Fondo slice reached HP1 conditions (at ~50 km depth). As described above, this tectonic slice included monometamorphic metasediments (Scalaro Unit), polymetamorphic rocks of the Bonze Unit and probably some of the metasediments belonging to the intermediate unit described by Venturini (1995). The intermediate unit is not shown separately, and is represented here as part of the EMC. For the sake of simplicity, the Fondo slice is shown in Fig. 15 as consisting only of Scalaro metasediments.

At ~68 Ma the Druer slice recorded a first stage of exhumation (medium-pressure stage) at blueschist-facies conditions at ~50 km depth (Fig. 15). At the same time, the rocks belonging to the Fondo slice recorded a medium-pressure stage (at ~35 km depth), presumably as they were being dragged up by the exhuming EMC.

At ~65 Ma faster subduction started in the Gneiss Minuti Complex (HP stage at ~45 Ma; e.g. Inger *et al.*, 1996; Cortiana *et al.*, 1998). The Fondo slice was therefore pulled down by the GMC, reaching the second HP stage at ~50 km, while the Eclogitic Micaschist Complex (as recorded by the Druer slice) continued exhuming slowly (~40 km depth).

Comparing the P–T–t paths for the Druer and Fondo slices with the record reported in previous studies for various areas of the EMC, it is increasingly evident that the Sesia Zone is composed of several tectonic fragments, which were independently mobile (in space and time) during the Cretaceous convergence. Although many details of the kinematics in the subduction channel are still missing, the scale of tectonic mobility (at least its vertical component) and the rates of such mixing processes are now resolved.

Our petrochronological approach thus yields field-based constraints on the duration and rates of the dynamics within a subduction channel. Different P–T paths for subduction-related metamorphic complexes, rather than a single P–T trajectory, are predicted by numerical models (e.g. Gerya *et al.*, 2002; Roda *et al.*, 2012). Complex subduction scenarios in which different HP slices are closely associated are emerging for other localities such as Alpine Corsica (Vitale Brovarone *et al.*, 2013) and the Kokchetav Complex (Stepanov, 2012). In these cases, however, nearby slices are distinguished on the basis of their different P–T paths and peak metamorphic conditions, but differences in timing were not recognized. In the case of the Sesia Zone, we demonstrate that slices having similar peak metamorphic conditions had a diachronous evolution in the subduction channel for which the detailed timing is now known.

ACKNOWLEDGEMENTS

P. Manzotti and G. Venturini are thanked for discussions and help with the fieldwork. Fruitful discussions with M. Robyr, J. Hermann, I. Mercolli, R. Compagnoni, B. Von

Niederhäusern and C. deCapitani led to improvements in this paper. B. Dhuime is thanked for technical assistance and Pb-isotope analyses. The constructive comments of three anonymous journal reviewers improved the final version of the paper. We thank R. Gieré for careful editorial handling.

FUNDING

This work was financed by Schweizerischer Nationalfonds (Swiss SNF Grants no. 200020_126946 and 146175).

SUPPLEMENTARY DATA

Supplementary data for this paper are available at *Journal of Petrology* online.

REFERENCES

Armstrong, J. T. (1988). Quantitative analysis of silicate and oxide materials: comparison of Monte Carlo, ZAF and φ(ρZ) procedures. In: Newbury, D. E. (ed.) *Microbeam Analysis*. San Francisco Press, pp. 239–246.

Armstrong, J. T. (1991). Quantitative elemental analysis of individual microparticles with electron beam instruments. In: Heinrich, K. F. J. & Newbury, D. E. (eds) *Electron Probe Quantitation*. Plenum, pp. 261–315.

Babist, J., Handy, M. R., Konrad-Schmolke, M. & Hammerschmidt, K. (2006). Precollisional, multistage exhumation of subducted continental crust: The Sesia Zone, western Alps. *Tectonics* **25**, TC6008.

Berman, R. G. (1988). Internally-consistent thermodynamic data for minerals in the system Na_2O–K_2O–CaO–MgO–FeO–Fe_2O_3–Al_2O_3–SiO_2–TiO_2–H_2O–CO_2. *Journal of Petrology* **29**, 445–522.

Black, L. P., Kamo, S. L., Allen, C. M., Aleinikoff, J. M., Davis, D. W., Korsch, R. J. & Foudoulis, C. (2003). TEMORA 1: a new zircon standard for Phanerozoic U–Pb geochronology. *Chemical Geology* **200**, 155–170.

Bussy, F., Venturini, G., Hunziker, J. & Martinotti, G. (1998). U–Pb ages of magmatic rocks of the western Austroalpine Dent-Blanche–Sesia unit. *Schweizerische Mineralogische und Petrographische Mitteilungen* **78**, 163–168.

Carswell, D. A., Brueckner, H. K., Cuthbert, S. J., Mehta, K. & O'Brien, P. J. (2003). The timing of stabilisation and the exhumation rate for ultra-high pressure rocks in the Western Gneiss region of Norway; petrochemical and tectonic processes of UHP/HP terranes II. *Journal of Metamorphic Geology* **21**, 601–612.

Cathelineau, M. (1988). Cation site occupancy in chlorites and illites as a function of temperature. *Clay Minerals* **23**, 471–485.

Compagnoni, R. (1977). The Sesia–Lanzo Zone: high pressure–low temperature metamorphism in the Austroalpine Continental Margin. *Rendiconti della Societá Italiana di Mineralogia e Petrologia* **33**, 335–374.

Compagnoni, R., Dal Piaz, G. V., Hunziker, J. C., Gosso, G., Lombardo, B. & Williams, P. F. (1977). The Sesia–Lanzo Zone, a slice of continental crust with Alpine high pressure–low temperature assemblages in the Western Italian Alps. *Rendiconti della Società Italiana di Mineralogia e Petrologia* **33**, 281–334.

Cortiana, G., Dal Piaz, G. V., Del Moro, A., Hunziker, J. C. & Martin, S. (1998). ^{40}Ar–^{39}Ar and Rb–Sr dating of the Pillonet klippe and the Sesia–Lanzo basal slice in the Ayas valley and evolution of the Austroalpine–Piedmont nappe stack. *Memorie di Scienze Geologiche* **50**, 177–194.

Dal Piaz, G. V., Hunziker, J. C. & Martinotti, G. (1972). La zona Sesia–Lanzo e l'evoluzione tettono-metamorfica delle Alpi Nordoccidentali interne. *Memorie della Società Geologica Italiana* **11**, 433–460.

Darbellay, B. (2009). Kinetics of crystal growth and equilibrium domains in eclogite of the Sesia Zone, Western Alps, Thèse de doctorat, Université de Lausanne, 142 pp.

Darling, J. R., Storey, C. D. & Engi, M. (2012*a*). Allanite U–Th–Pb geochronology by laser ablation ICPMS. *Chemical Geology* **292–293**, 103–115.

Darling, J. R., Storey, C. D., Hawkesworth, C. J. & Lightfoot, P. C. (2012*b*). *In-situ* Pb isotope analysis of Fe–Ni–Cu sulphides by laser ablation multi-collector ICPMS: New insights into ore formation in the Subdury impact melt sheet. *Geochimica et Cosmochimica Acta* **99**, 1–17.

de Capitani, C. & Brown, T. H. (1987). The computation of chemical equilibrium in complex systems containing non-ideal solutions. *Geochimica et Cosmochimica Acta* **51**, 2639–2652.

de Capitani, C. & Petrakakis, K. (2010). The computation of equilibrium assemblage diagrams with Theriak/Domino software. *American Mineralogist* **95(7)**, 1006–1016.

Dewey, J. F., Helman, M. L., Turco, E., Hutton, D. H. W. & Knott, S. D. (1989). Kinematics of the western Mediterranean. In: Coward, M. P., Dietrich, D. & Park, R. G. (eds) *Alpine Tectonics. Geological Society, London, Special Publications* **45**, 265–283.

Duchêne, S., Blichert-Toft, J., Luais, B., Télouk, P., Lardeaux, J. M. & Albarède, F. (1997). The Lu–Hf dating of garnets and the ages of the Alpine high-pressure metamorphism. *Nature* **387**, 586–589.

Ellis, D. J. & Green, D. H. (1979). An experimental study of the effect of Ca upon garnet–clinopyroxene Fe–Mg exchange equilibria. *Contribution to Mineralogy and Petrology* **71**, 13–22.

Ernst, W. G. (2001). Subduction, ultrahigh-pressure metamorphism, and regurgitation of buoyant crustal slices; implications for arcs and continental growth; processes and consequences of deep subduction. *Physics of the Earth and Planetary Interiors* **127**, 253–275.

Gabudianu Radulescu, I., Rubatto, D., Gregory, C. & Compagnoni, R. (2009). The age of the HP metamorphism in the Gran Paradiso Massif, Western Alps: A petrological and geochronological study of 'silvery micaschists'. *Lithos* **110**, 95–108.

Gatta, G. D., Rotiroti, N. & Zucali, M. (2009). Plastic deformations in kyanites by tectonometamorphic processes: a single-crystal X-ray diffraction study. *Mineralogical Magazine* **73**, 359–371.

Gerya, T. V., Stoeckhert, B. & Perchuk, A. L. (2002). Exhumation of high-pressure metamorphic rocks in a subduction channel; a numerical simulation. *Tectonics* **21**, 19, doi:10.1029/2002TC001406.

Ghent, E. D. & Stout, M. Z. (1984). TiO_2 activity in metamorphosed pelitic and basic rocks—principles and applications to metamorphism in southeastern Canadian cordillera. *Contributions to Mineralogy and Petrology* **86**, 248–255.

Gosso, G. (1977). Metamorphic evolution and fold history in the eclogite micaschists of the upper Gressoney valley (Sesia–Lanzo zone, Western Alps). *Rendiconti della Società Italiana di Mineralogia e Petrologia* **33**, 389–407.

Gottschalk, M. (2004). Thermodynamic properties of zoisite, clinozoisite and epidote. In: Liebscher, A. & Franz, G. (eds) *Epidotes. Mineralogical Society of America and Geochemical Society Reviews in Mineralogy and Geochemistry* **56**, 83–124.

Green, T. H. & Hellman, P. L. (1982). Fe–Mg partitioning between coexisting garnet and phengite at high pressure, and comments on a garnet–phengite geothermometer. *Lithos* **4**, 253–266.

Gregory, C. J., Rubatto, D., Allen, C. M., Williams, I. S., Hermann, J. & Ireland, T. (2007). Allanite micro-geochronology: A LA-ICP-MS and SHRIMP U–Th–Pb study. *Chemical Geology* **245**, 162–182.

Guillong, M., Meier, D. M., Allan, M. M., Heinrich, C. A. & Yardley, B. (2008). Appendix A6: SILLS: A MATLAB-based program for the reduction of laser ablation ICP–MS data of homogeneous materials and inclusions. In: Sylvester, P. (ed.) *Mineralogical Association of Canada, Short Course Series. Laser Ablation ICP-MS in the Earth Sciences: Current Practices and Outstanding Issues*. Vancouver, B.C. **40**, 328–333.

Handy, M. R., Schmid, S. M., Bousquet, R., Kissling, E. & Bernoulli, D. (2010). Reconciling plate-tectonic reconstructions of Alpine Tethys with the geological–geophysical record of spreading and subduction in the Alps. *Earth-Science Reviews* **102**, 121–158.

Hermann, J. & Rubatto, D. (2003). Relating zircon and monazite domains to garnet growth zones: age and duration of granulite facies metamorphism in the Val Malenco lower crust. *Journal of Metamorphic Geology* **21**, 833–852.

Horn, I., Hilton, R. W., Jackson, S. E. & Longerich, H. P. (1997). Ultra-trace element analysis of NIST SRM 616 and 614 using laser ablation microprobe-inductively coupled plasma-mass spectrometry (LAM-ICP-MS): a comparison with secondary ion mass spectrometry (SIMS). *Geostandards and Geoanalytical Research* **21**, 191–203.

Hunziker, J. C. (1974). Rb–Sr and K–Ar age determination and the Alpine history of the Western Alps. *Memorie degli Istituti di Geologia e Mineralogia dell'Universitá di Padova* **31**, 1–54.

Inger, S., Ramsbotham, W., Cliff, R. A. & Rex, D. C. (1996). Metamorphic evolution of the Sesia–Lanzo Zone, Western Alps: Time constraints from multi-system geochronology. *Contributions to Mineralogy and Petrology* **126**, 152–168.

Janots, E., Engi, M., Berger, A., Allaz, J., Schwarz, J. O. & Spandler, C. (2008). Prograde metamorphic sequence of REE minerals in pelitic rocks of the Central Alps: implications for allanite–monazite–xenotime phase relations from 250 to 610°C. *Journal of Metamorphic Geology* **26**, 509–526.

Konrad-Schmolke, M., O'Brien, P. & Zack, T. (2011). Fluid migration above a subducted slab—constraints on amount, pathways and major element mobility from partially overprinted eclogite-facies rocks (Sesia Zone,Western Alps). *Journal of Petrology* **52**, 457–486.

Kurz, W. & Froitzheim, N. (2002). The exhumation of eclogite-facies metamorphic rocks; a review of models confronted with examples from the Alps. *International Geology Review* **44**, 702–743.

Lardeaux, J. M. & Spalla, M. I. (1991). From granulites to eclogites in the Sesia zone (Italian Western Alps): a record of the opening and closure of the Piedmont ocean. *Journal of Metamorphic Geology* **9**, 35–59.

Lardeaux, J.-M., Gosso, G., Kienast, J.-R. & Lombardo, B. (1982). Relations entre le metamorphisme et la déformation dans la zone Sesia–Lanzo (Alpes Occidentales) et le problème de l'éclogitisation de la croûte continentale. *Bulletin de la Société Géologique de France* **24**, 793–800.

Ludwig, K. R. (2003). *Isoplot/Ex version 3.0. A geochronological toolkit for Microsoft Excel. Berkeley Geochronological Centre Special Publications* **4**, .

Mancktelow, N. S. (2008). Tectonic pressure: Theoretical concepts and modelled examples. *Lithos* **103**, 149–177.

Marmo, B. A., Clarke, G. L. & Powell, R. (2002). Fractionation of bulk rock composition due to porphyroblast growth: effects on eclogite facies mineral equilibria, Pam Peninsula, New Caledonia. *Journal of Metamorphic Geology* **20**, 151–165.

Mukherjee, B. K., Sachan, H. K., Ogasawara, Y., Muko, A. & Yoshioka, N. (2003). Carbonate-bearing UHPM rocks from the Tso–Morari region, Ladakh, India; petrological implications. *International Geology Review* **45**, 49–69.

Oberhänsli, R., Hunziker, J. C., Martinotti, G. & Stern, W. B. (1985). Geochemistry,geochronology and petrology of Monte Mucrone: an example of Eo-Alpine eclogitization of Permian granitoids in the Sesia–Lanzo zone, western Alps, Italy. *Chemical Geology* **52**, 165–184.

Okamoto, A. & Toriumi, M. (2004). Optimal mixing properties of calcic and subcalcic amphiboles: application of Gibbs' method to the Sanbagawa schist, SW Japan. *Contributions to Mineralogy and Petrology* **146**, 529–545.

Parrish, R. R., Gough, S. J., Searle, M. P. & Waters, D. J. (2006). Plate velocity exhumation of ultrahigh-pressure eclogites in the Pakistan Himalaya. *Geology* **34**, 989–992.

Passchier, C. W., Urai, J. L., Van Loon, J. & Williams, P. F. (1981). Structural geology of the central Sesia–Lanzo Zone. *Geologie en Mijnbouw* **60**, 497–507.

Pearce, N. J. G., Perkins, W. T., Westgate, J. A., Gorton, M. P., Jackson, S. E., Neal, C. R. & Chenery, S. P. (1997). A compilation of new and published major and trace element data for NIST SRM 610 and NIST SRM 612 glass reference materials. *Geostandards and Geoanalytical Research* **21**, 115–144.

Petrík, I., Broska, I., Lipka, J. & Siman, P. (1995). Granitoid allanite-(Ce): substitution relations, redox conditions and REE distributions (on an example of I-type granitoids, Western Carpathians, Slovakia). *Geologica Carpathica* **46**, 79–94.

Platt, J. P. (1993). Exhumation of high-pressure rocks; a review of concepts and processes. *Terra Nova* **5**, 119–133.

Pognante, U. (1989). Tectonic implications of lawsonite formation in the Sesia zone (Western Alps). *Tectonophysics* **162**, 219–227.

Powell, R. (1985). Regression diagnostics and robust regression in geothermometer/geobarometer calibration: the garnet–clinopyroxene geothermometer revisited. *Journal of Metamorphic Geology* **3**, 231–243.

Rebay, G. & Spalla, M. I. (2001). Emplacement at granulite facies conditions of the Sesia–Lanzo metagabbros: an early record of Permian rifting? *Lithos* **58**, 85–104.

Reinsch, D. (1979). Glaucophanites and eclogites from Val Chiusella, Sesia–Lanzo Zone (Italian Alps). *Contributions to Mineralogy and Petrology* **70**, 257–266.

Roda, M., Marotta, A. M. & Spalla, M. I. (2010). Numerical simulations of an ocean/continent convergent system: influence of subduction geometry and mantle wedge hydration on crustal recycling. *Geochemistry, Geophysics, Geosystems* **11**, Q05008, doi:10.1029/2009GC003015.

Roda, M., Spalla, M. I. & Marotta, A. M. (2012). Integration of natural data within a numerical model of ablative subduction: a possible interpretation for the Alpine dynamics of the Austroalpine crust. *Journal of Metamorphic Geology* , doi:10.1111/jmg.12000.

Rubatto, D. (2002). Zircon trace element geochemistry: partitioning with garnet and the link between U–Pb ages and metamorphism. *Chemical Geology* **184**, 123–138.

Rubatto, D. & Hermann, J. (2001). Exhumation as fast as subduction? *Geology* **29**, 3–6.

Rubatto, D. & Hermann, J. (2003). Zircon formation during fluid circulation in eclogites (Monviso, Western Alps): Implications for Zr and Hf budget in subduction zones. *Geochimica and Cosmochimica Acta* **67**, 2173–2187.

Rubatto, D. & Hermann, J. (2007). Experimental zircon/melt and zircon/garnet trace element partitioning and implications for the geochronology of crustal rocks. *Chemical Geology* **241**, 38–61.

Rubatto, D., Gebauer, D. & Compagnoni, R. (1999). Dating of eclogite facies zircons: the age of Alpine metamorphism in the Sesia–Lanzo Zone (Western Alps). *Earth and Planetary Science Letters* **167**, 141–158.

Rubatto, D., Regis, D., Hermann, J., Boston, K., Engi, M., Beltrando, M. & McAlpine, S. R. B. (2011). Yo-yo subduction recorded by accessory minerals in the Sesia Zone, Western Alps. *Nature Geoscience* **4**, 338–342.

Ruffet, G., Gruau, G., Ballèvre, M., Feraud, G. & Philippot, P. (1997). Rb–Sr and ^{40}Ar–^{39}Ar laser probe dating of high-pressure phengites from the Sesia zone (Western Alps): Underscoring of excess argon and new age constraints on the high-pressure metamorphism. *Chemical Geology* **141**, 1–18.

Scherrer, N. C., Engi, M., Gnos, E., Jakob, V. & Liechti, A. (2000). Monazite analysis; from sample preparation to microprobe age dating and REE quantification. *Schweizerische Mineralogische und Petrographische Mitteilungen* **80**, 93–105.

Sláma, J., Košler, J., Condon, D. J., Crowley, J. L., Gerdes, A., Hanchar, J. M., Horstwood, M. S. A., Morris, G. A., Nasdala, L., Norberg, N., Schaltegger, U., Schoene, B., Tubrett, M. N. & Whitehouse, M. J. (2008). Plešovice zircon—A new natural reference material for U–Pb and Hf isotopic microanalysis. *Chemical Geology* **249**, 1–35.

Smye, A. J., Greenwood, L. V. & Holland, T. J. B. (2010). Garnet–chloritoid–kyanite assemblages: eclogite facies indicators of subduction constraints in orogenic belts. *Journal of Metamorphic Geology* **28**, 753–768.

Spalla, M. I. & Zulbati, F. (2003). Structural and petrographic map of the southern Sesia–Lanzo Zone; Monte Soglio–Rocca Canavese, Western Alps, Italy. *Memorie di Scienze Geologiche* **55**, 119–127.

Spalla, M. I., Zucali, M., Di Paola, S. & Gosso, G. (2005). A critical assesment of the tectono-thermal memory of rocks and definition of the tectonometamorphic units: evidence from fabric and degree of metamorphic transformations. In: Gapais, D., Brun, J. P. & Cobbold, P. (eds) *Deformation Mechanisms, Rheology and Tectonics: From Minerals to the Lithosphere. Geological Society, London, Special Publications* **243**, 227–247.

Stacey, J. S. & Kramers, J. D. (1975). Approximation of terrestrial lead evolution by a two-stage model. *Earth and Planetary Science Letters* **26**, 207–221.

Stepanov, A. S. (2012). Monazite control on Th, U, and REE redistribution during partial melting: experiments and application to deeply subducted crustResearch School of Earth Sciences, Canberra, Australian National University, PhD Thesis, 247 p.

Stoeckhert, B. & Gerya, T. V. (2005). Pre-collisional high pressure metamorphism and nappe tectonics at active continental margins; a numerical simulation. *Terra Nova* **17**, 102–110.

Stoeckhert, B., Jaeger, E. & Voll, G. (1986). K–Ar determinations on phengites from the internal part of the Sesia Zone, Western Alps. *Contributions to Mineralogy and Petrology* **92**, 456–470.

Sun, S. S. & McDonough, W. F. (1989). Chemical and isotopic systematic of oceanic basalts: implications for mantle composition and processes. In: Saunders, A. D. & Norry, M. J. (eds) *Magmatism in the Ocean Basins. Geological Society, London, Special Publications* **42**, 313–345.

Terry, M. P., Robinson, P., Hamilton, M. A. & Jercinovic, M. J. (2000). Monazite geochronology of UHP and HP metamorphism, deformation, and exhumation, Nordoyane, Western Gneiss region, Norway. *American Mineralogist* **85**, 1651–1664.

Tropper, P. & Essene, E. J. (2002). Thermobarometry in eclogites with multiple stages of mineral growth: an example from the Sesia–Lanzo Zone (Western Alps, Italy). *Schweizerische Mineralogische und Petrographische Mitteilungen* **82**, 487–514.

Venturini, G. (1995). Geology, geochemistry and geochronology of the inner central Sesia Zone (Western Alps, Italy). *Mémoires de Géologie (Lausanne)*, PhD Thesis **25**, 148.

Vidal, O., Parra, T. & Trotet, F. (2001). A thermodynamic model for Fe–Mg aluminous chlorite using data from phase equilibrium experiments and natural pelitic assemblages in the 100–600°C, 1–25 kbar range. *American Journal of Science* **63**, 557–592.

Vidal, O., Parra, T. & Vieillard, P. (2005). Thermodynamic properties of the Tschermak solid solution in Fe-chlorites: Application to natural examples and possible role of oxidation. *American Mineralogist* **90**, 359–370.

Vidal, O., DeAndrade, V., Lewin, E., Munoz, M., Parra, T. & Pascarelli, S. (2006). *P–T*–deformation–Fe^{3+}/Fe^{2+} mapping at the thin section scale and comparison with XANES mapping. Application to a garnet-bearing metapelite from the Sambagawa metamorphic belt (Japan). *Journal of Metamorphic Geology* **24**, 669–683.

Vitale Brovarone, A., Beyssac, O., Malavieille, J., Molli, G., Beltrando, M. & Compagnoni, R. (2013). Stacking and metamorphism of continuous segments of subducted lithosphere in a high-pressure wedge: The example of Alpine Corsica (France). *Earth-Science Reviews* **116(1)**, 35–56.

von Blanckenburg, F. (1992). Combined high-precision chronometry and geochemical tracing using accessory minerals: Applied to the Central-Alpine Bergell intrusion (central Europe). *Chemical Geology* **100**, 19–40.

Vuichard, J. P. (1989). La marge Austroalpine durant la collision Alpine: Evolution tectonometamorphique de la zone Sesia Lanzo, Doctoral thesis, Rennes, 3ème cycle, 307 pp.

Warren, C. J., Beaumont, C. & Jamieson, R. A. (2008). Modelling tectonic styles and ultra-high pressure (UHP) rock exhumation during the transition from oceanic subduction to continental collision. *Earth and Planetary Science Letters* **267**, 129–145.

Warren, C. J., Grujic, D., Kellett, D. A., Cottle, J., Jamieson, R. A. & Ghalley, K. S. (2011). Probing the depths of the India–Asia collision: U–Th–Pb monazite chronology of granulites from NW Bhutan. *Tectonics* **30**, TC2004, doi:10.1029/2010TC002738.

Waters, D. J. & Martin, H. N. (1993). Geobarometry in phengite-bearing eclogites. *Terra Abstracts* **5**, 410–411.

Watson, E. B., Wark, D. A. & Thomas, J. B. (2006). Crystallization thermometers for zircon and rutile. *Contributions to Mineralogy and Petrology* **151**, 413–433.

Whitney, D. L. & Evans, B. W. (2010). Abbreviations for names of rock-forming minerals. *American Mineralogist* **95**, 185–187.

Williams, I. S. (1998). U–Th–Pb geochronology by ion microprobe. In: McKibben, M. A., Shanks, W. C., III & Ridley, W. I. (eds) *Application of Microanalytical Techniques to Understanding Mineralizing Processes*, Reviews in Economic Geology, Society of Economic Geologist **7**, 1–35.

Williams, P. F. & Compagnoni, R. (1983). Deformation and metamorphism in the Bard area of the Sesia–Lanzo Zone, Western Alps, during subduction and uplift. *Journal of Metamorphic Geology* **1**, 117–140.

Zucali, M. (2002). Foliation map of the 'Eclogitic Micaschist Complex' (Monte Mucrone–Monte Mars–Mombarone, Sesia–Lanzo Zone, Italy). *Memorie di Scienze Geologiche* **54**, 87–100.

Zucali, M. & Spalla, M. I. (2011). Prograde lawsonite during the flow of continental crust in the Alpine subduction: Strain vs. metamorphism partitioning, a field-analysis approach to infer tectono-metamorphic evolutions (Sesia–Lanzo Zone, Western Italian Alps). *Journal of Structural Geology* **33**, 381–398.

Zucali, M., Spalla, M. I. & Gosso, G. (2002). Strain partitioning and fabric evolution as a correlation tool: the example of the Eclogitic Micaschists Complex in the Sesia–Lanzo Zone (Monte Mucrone–Monte Mars, Western Alps, Italy). *Schweizerische Mineralogische und Petrographische Mitteilungen* **82**, 429–454.

Zucali, M., Spalla, M. I., Gosso, G., Racchetti, S. & Zulbati, F. (2004). Prograde LWS–KY transition during subduction of the Alpine continental crust of the Sesia–Lanzo Zone: the Ivozio Complex. *Journal of Virtual Explorer* **16**, paper 4.